Mesoscale patterns in the Cape São Vicente (Iberian Peninsula) upwelling region

Paulo Relvas

Centro de Investigação Marinha e Ambiental, Universidade do Algarve, Faro, Portugal

Eric D. Barton

School of Ocean Sciences, University of Wales, Menai Bridge, UK

[1]   The coastal upwelling region near Cape São Vicente, the southwestern tip of the Iberian Peninsula where the southern zonal coast meets the meridional western coast, was studied using over 1200 advanced very high resolution radiometer (AVHRR) satellite images of sea surface temperature and time series of sea level height, wind velocities, and nearshore sea surface temperature recorded at coastal sites within 200 km of the cape. Summer upwelling is more intense and persistent off the western coast than off the southern coast, where a recurrent warm coastal countercurrent flows westward, and at times turns northward along the western coast after reaching the cape. In this region the equatorward current jet of cold water upwelled off the western coast is no longer bounded by a coast. Three preferred directions for the spreading of this water are identified. The most persistent is eastward along the southern shelf break and slope, possibly merging with waters previously upwelled locally, which becomes separated from shore by the coastal progression of the warmer counterflow. The second preferred direction results in the southward development of a cold filament feature fed by cold waters upwelled farther north and represents the southernmost extent of the intense coastal upwelling jet, which overshoots the cape. The least frequent feature to develop is a cold filament that grows westward at the latitude of the cape, appearing to result from the meandering of the equatorward jet. The coastal countercurrent is seen to interact with the equatorward jet at times of relaxation, not only by separating the cold upwelled water from the coast but, when it is energetic enough, breaking westward offshore through the equatorward cold flow and separating the eastward and southward cold features from the upcoast cold waters. Empirical evidence shows the presence of an alongshore pressure gradient, stronger in summer, driving the coastal progression of the warm counterflow. Wind forcing plays an important role in the circulation by augmenting or diminishing the effect of the preexisting alongshore pressure gradients. The extent of the progression of the warm coastal countercurrent along the southern and western coast is dictated by the the strength of the upwelling favorable wind stress, which is able to balance and reverse the alongshore flow, at least in the upper layers.   INDEX TERMS: 4223 Oceanography: General: Descriptive and regional oceanography; 4279 Oceanography: General: Upwelling and convergences; 4516 Oceanography: Physical: Eastern boundary currents; 4520 Oceanography: Physical: Eddies and mesoscale processes; 4572 Oceanography: Physical: Upper ocean processes; KEYWORDS: Iberian Peninsula, eastern boundaries, transition zone, cold filaments, coastal countercurrents, sea level

1.   Introduction

[2]   The Iberian Peninsula forms the northern extremity of the eastern boundary of the North Atlantic subtropical gyre, situated between the equatorward flowing surface Canary Current and the northeastward flowing North Atlantic Current. Cape São Vicente represents the southern limit of the Iberian upwelling (Figure 1), which is separated from the NW African upwelling by the Gulf of Cádiz and entrance of the Mediterranean. At the cape, the western and southern coasts of Iberia intersect at almost right angles. The ≈25 km wide southern shelf slopes gently down to a sharp edge at 100–130 meters depth, defined by a sudden step down to the 700 m contour. This pronounced feature extends around the southwest tip of
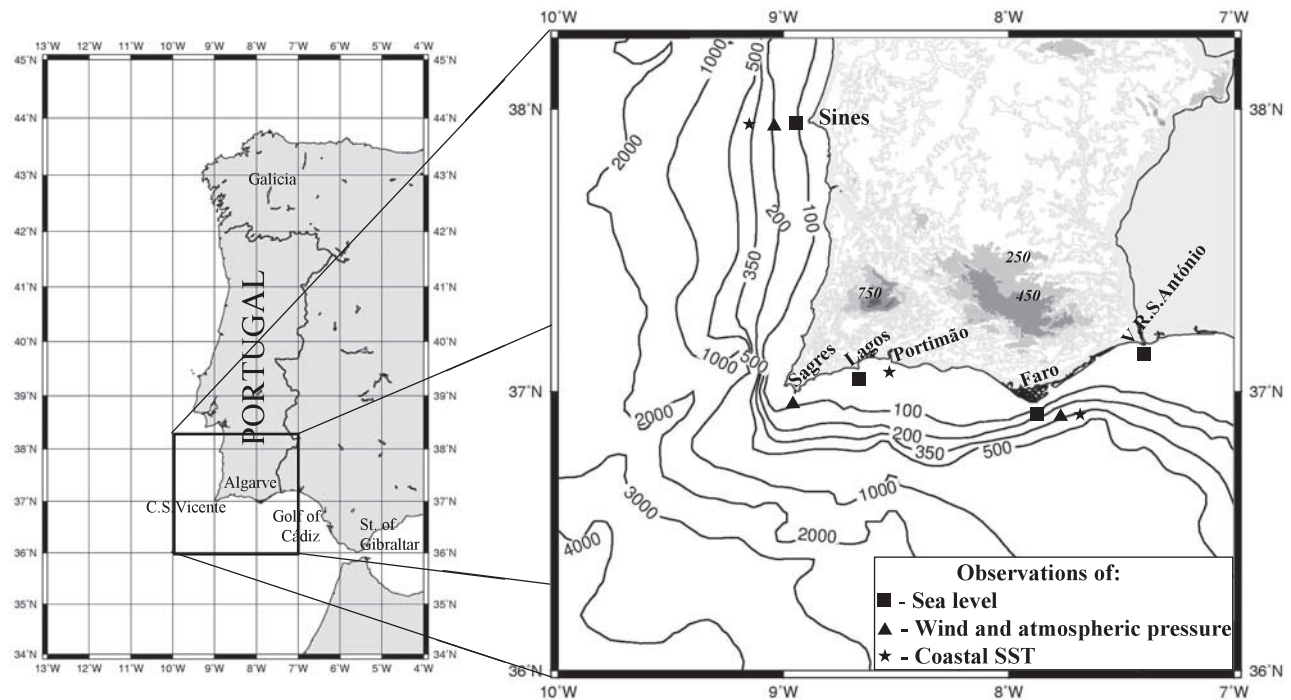
Figure 1. General bathymetry and coastal morphology of Iberian region. Contours are in meters. The locations where the time series were taken are shown in the inset.

Portugal, reaching about 10 km north of Cape São Vicente. The shelf off the west coast of Algarve is steep and only ≈10 km wide.

[3] The coastal transition zone off Iberia is characterized by a marked seasonality related to the large-scale wind climatology. Both satellite imagery and in situ observations reveal a surface poleward current as a persistent feature of the winter circulation, when winds relax or are downwelling favorable [*Frouin et al.*, 1990; *Haynes and Barton*, 1990]. A well-defined upwelling season between March and September [*Wooster et al.*, 1976; *Fiúza et al.*, 1982] results from strong northerly winds associated with the northward displacement of the Açores high-pressure cell and the weakening of the Iceland low. Upwelling causes the surface dynamic height to decrease toward the coast and the resulting equatorward geostrophic current is enough to counter the poleward slope current at and near the surface, establishing a southward flow. However, the deeper waters, below 100–200 m, still flow poleward as an undercurrent advecting waters of predominantly subtropical and Mediterranean origin [*Haynes and Barton*, 1990]. Along the south coast, the summer wind pattern is affected by the establishment of a low pressure centre of thermal origin over the Iberian Peninsula, which causes eastward wind off southern Portugal.

[4] During the upwelling season the temperature front along the west coast that separates cooler, recently upwelled water from offshore oceanic water is generally populated with cool filaments [*Sousa and Bricaud*, 1992; *Haynes et al.*, 1993]. These are narrow contorted tongues of cooler upwelled water extending hundreds of kilometers seaward from the coastal zone [*Brink and Cowles*, 1991]. Off Iberia filaments are associated with major topographic features, in particular, prominent capes; Cape São Vicente is the origin of a major filament [*Haynes et al.*, 1993]. At different times this filament extends in different directions, even eastward into the Gulf of Cádiz, unlike the other filaments which extend generally westward.

[5] Often, a coastal countercurrent carries warm surface waters to the west, close to the Algarve shore, on occasion turning clockwise around Cape São Vicente to flow poleward along the west coast [*Fiúza*, 1982]. This feature coincides with periods of weak winds along the south coast, when it interacts with the colder waters previously upwelled. Inshore poleward countercurrents also are a persistent feature of the Californian continental margin during the upwelling season [e.g., *Kosro*, 1987; *Chelton et al.*, 1988; *Huyer et al.*, 1989]. They have been most commonly attributed to a favorable pattern of the wind stress curl near the coast [*McCreary et al.*, 1987; *Bray et al.*, 1999; *Oey*, 1999] or to an alongshore pressure gradient that opposes the upwelling favorable wind stress [*Hickey and Pola*, 1983; *Winant et al.*, 1987; *Ramp and Abbott*, 1998].

[6] In this paper the variability and kinematics of the mesoscale field of the coastal transition zone off Cape São Vicente during the upwelling season, observed from advanced very high resolution radiometer (AVHRR) satellite imagery, are described. In particular, the formation, evolution, and persistence of the Cape São Vicente filament and the contrasting generation of the warm coastal poleward counterflow are studied. Wind, sea level, and nearshore sea surface temperature data are used to analyze the possible forcing mechanisms associated with these mesoscale features. The occurrence of an alongshore pressure gradient along southern Iberia is examined and the relation between different flow regimes and wind stress

and pressure gradient forcing is discussed by means of momentum analysis.

2. Observations

2.1. Satellite Data and Processing

[7] The AVHRR sea surface temperature satellite data used in this investigation were collected onboard the NOAA series polar orbiting satellites. The ground resolution provided by these satellites is 1.1 km × 1.1 km at nadir increasing to 2.5 km × 7.0 km at maximum scan angles. Satellite data include an archive of over 1200 monochrome prints representing brightness temperature scenes of relatively cloud-free AVHRR images provided by the University of Dundee satellite ground receiving station, for the period 1981–1995. This photographic form allowed only a qualitative analysis of the temperature patterns, and so 35 images of particular interest were obtained in digital form from the University of Dundee. These were processed at the NERC Remote Sensing Data Analysis Service, Plymouth Marine Laboratory, UK, using the semiautomated *Panorama* (Processing and Automatic Navigation Of ReAl-time iMAges) satellite image processing system [*Miller et al.*, 1996], and then edited for attributes, annotations, and composition at University of Algarve, Portugal, allowing a quantitative analysis of the sea surface temperature fields.

[8] The AVHRR is a scanning radiometer sensitive in five spectral channels, two of them (channel 1 and 2) operating in the visible wavelengths. The radiance measured by the sensors is directly related to the sea surface temperature. For the determination of sea surface temperatures only the infrared channels 4 (10.3–11.3 μm) and 5 (11.5–12.5 μm) are used in the atmospheric correction algorithm. However, in satellites NOAA 6,7,8, and 10 the AVHRR channel 5 is a copy of the channel 4 sensor, and therefore existing atmospheric correction algorithms were not considered reliable enough for the computation of the sea surface temperature. Images from these satellites were calibrated only for channel 4 brightness temperature, as a rough indication of temperature gradients and differences across the area of the sea being viewed. The atmospheric correction was performed using the split window algorithm of *McClain et al.* [1985], which combines the brightness temperatures for channels 4 and 5.

2.2. Coastal Observations

[9] Sea level data recorded hourly from January 1982 to December 1991 at four tide gauges, located at Sines in the west coast and at Lagos, Faro, and V.R.S. António along the south coast (Figure 1), were obtained from Instituto Hidrográfico, Lisbon, which is responsible for the national tide-gauge chain. Unfortunately, none of the tide gauges provided a complete time series. Faro tide gauge had three consecutive years of records, but suffered a significant instrumental drift. The data set was not used for seasonal and mean analysis of sea level height, only for short term analysis. The hourly time series were split into sets without gaps and filtered to eliminate tidal and higher frequencies by means of a Cosine-Lanczos low-pass filter with half power point at 40 hours (0.6 cpd) spanning 121 hours. The time series data were then resampled at 6 hour intervals and small gaps in the data, typically less than 10 days, were filled with linearly interpolated data. Standard procedures of the Instituto Hidrográfico include the inspection of the tide gauge leveling. All tide gauges of the national net are leveled with a maximum error of 0.5 cm (personal communication from Instituto Hidrográfico), and all departures are referred to the national hydrographic zero. The hydrographic zero was defined by the Instituto Hidrográfico as the reference level for the tide gauge records and is located 2 m below the benchmark established for the country, so that it is below the lowest computed astronomic tide [*Hidrográfico*, 1996].

[10] Records of atmospheric pressure at Sines, Sagres and Faro (Figure 1), for the period 1980–1991, were obtained from the Instituto de Meteorologia, Lisbon. Sines station is located on the west coast at 16 m above mean sea level, Sagres station is on the Cape São Vicente cliffs at 38 m, and Faro station is on the seashore on the south coast, at 9 m. A reduction to the mean sea level of all the atmospheric pressure data was done using the hydrostatic equilibrium for a standard atmosphere ($\partial p/\partial z = -\rho g$ giving 1mbar ≈ 8 m in altitude). The absolute values of sea level pressure were similar in all three meteorological stations, and atmospheric pressure variations were basically the same at all stations, even for high frequencies. Thus, atmospheric pressure should not affect differences in sea level between tide gauges. The atmospheric pressure time series were then demeaned with the mean atmospheric pressure of the period 1960–1989 at each meteorological station, reduced to the mean sea level. The low-passed sea level time series were then combined with the contemporaneous atmospheric pressure residuals of the nearest meteorological station to correct for the inverted barometric effect. Distance between the tide gauge and the meteorological station was never larger than 100 km.

[11] Wind and nearshore sea surface temperature data were made available by courtesy of the Instituto de Meteorologia, Lisbon. Wind data were recorded every hour at Faro, every 3 hours at Sagres and every 8 hours at Sines. The nearshore surface temperature was collected every day at Sines, at Portimão, on the western part of the south coast, and at Faro (Figure 1). Data were collected directly from the seashore, in shallow water, at 0900 LT every morning, in order to avoid the effect of the daily heating cycle. For the present analysis, periods less than 40 hours were filtered from the wind and temperature series.

3. Interannual Variability of Mesoscale Features

[12] A detailed and systematic analysis of all (over 900) cloud-free images from the AVHRR imagery archive between 1982 and 1991 was carried out. Most were collected between May and October. Image analysis was limited to the region 35°30′–38°30′N and 10°30′–7°00′W, the Cape São Vicente region. It was possible to identify separately the temporal evolution of four particular mesoscale features of the sea surface temperature field of the region: west coast upwelling, south coast upwelling, Cape São Vicente upwelling filament, and south coast countercurrent.

[13] The seasonal evolution of these features is represented in Figure 2, along with the record of cloud-free AVHRR images. These features occur mainly during summertime. Imagery collected during winter time shows a mostly uniform sea surface temperature field.
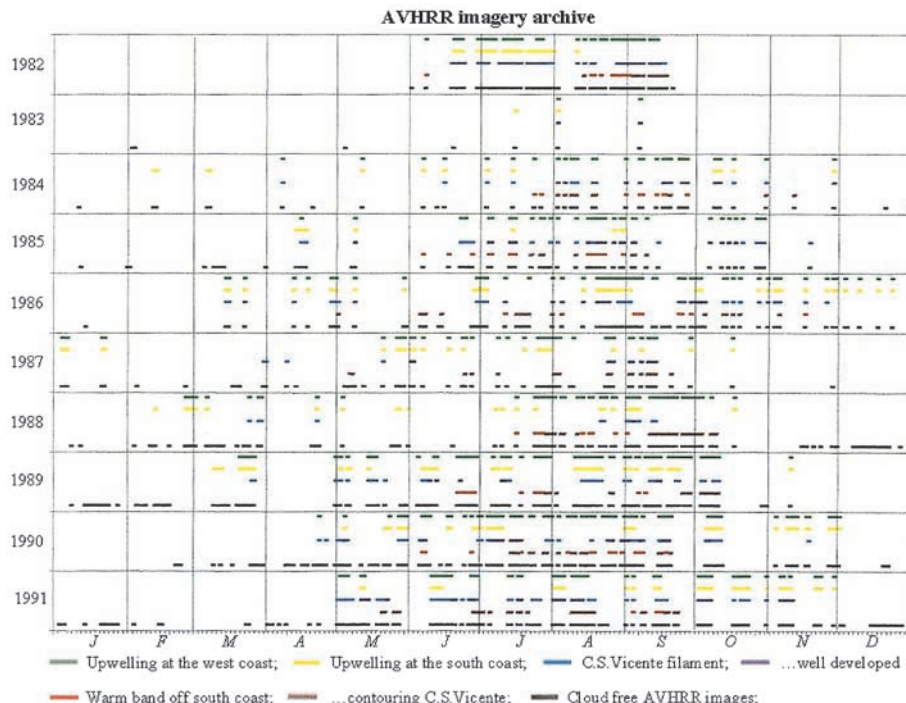
Figure 2. Evolution of the main features of the sea surface temperature field in the Cape São Vicente region between 1982 and 1991. Information about the sampled AVHRR images is also displayed.

[14] Figure 2 shows that the frequency of occurrence of upwelling in the south coast is 50% of the upwelling occurrences in the west coast. Also, west coast upwelling is concentrated in the summer months, while in the south coast upwelling events are more distributed through the year. The south coast upwelling is, mainly, most intense or limited to near Cape São Vicente. The development of upwelling conditions farther east than Cape Santa Maria (Faro) is sporadic (less than 10% of the south coast upwelling events).

[15] The Cape São Vicente filament, with various orientations, is a frequent feature from late Spring till early Autumn (80% of clear images between May and October). However, the filament is intermittent, and its continuous presence during the entire season is exceptional. Its initial development is associated with the establishment of upwelling in the west coast, and its continued growth requires persistence of upwelling. This leads to the hypothesis that the filament is primarily fed by waters upwelled farther north and advected equatorward by the coastal jet associated with the upwelling. However, upwelling on the west coast can occur without growth of the filament, as observed during part of the summers of 1987 and 1989 and almost all the summer of 1988. Figure 2 reveals that the development and decay of the Cape São Vicente filament is independent of the occurrence of upwelling in the Algarve coast, suggesting that the filament is not supplied by the water upwelled there.

[16] One of the most recurrent features, that occurs in 45% of clear images during the period of stronger coastal activity (end of May/June till October), is the development of a narrow band of warm water along the south coast of Algarve, leaving cooler water offshore over the continental slope. Figure 2 shows that this coastal warm feature develops whenever coastal upwelling is absent from the south coast. Satellite imagery shows the westward progression of this warm band along the Algarve begins in the east, near the Gulf of Cádiz, where a pool of warm surface water is found. *Folkard et al.* [1997] reported the pool generally shifted more westward when the prevailing wind in the gulf develops an easterly component. Sometimes, when upwelling is absent for a long period (typically more than 10 days), this warm feature turns around Cape São Vicente and extends poleward. In extreme conditions, the warm water can reach the Cape of Sines, about 100 km to the north.

[17] The presence of this coastal warm feature is somewhat independent of the presence of the Cape São Vicente filament. If the filament is present when the warm water reaches the Cape São Vicente, then the cool west coast upwelling jet that supplies the filament is forced to separate from the coast, and the filament loses its connection with the cape, being apparently fed with cooler water upwelled farther north.

4. Coastal Observations and Mesoscale Features

[18] Measurements of wind, sea level, and nearshore sea surface temperature during summer 1982, were analyzed together with the AVHRR imagery. This period was chosen because it shows development of a typical mesoscale pattern and an excellent set of observations were available. Upwelling along the west coast, development of the Cape São Vicente filament and the setup and progression of the band of warm water along the southwest coast were all observed. The time series are represented in Figure 3, with a
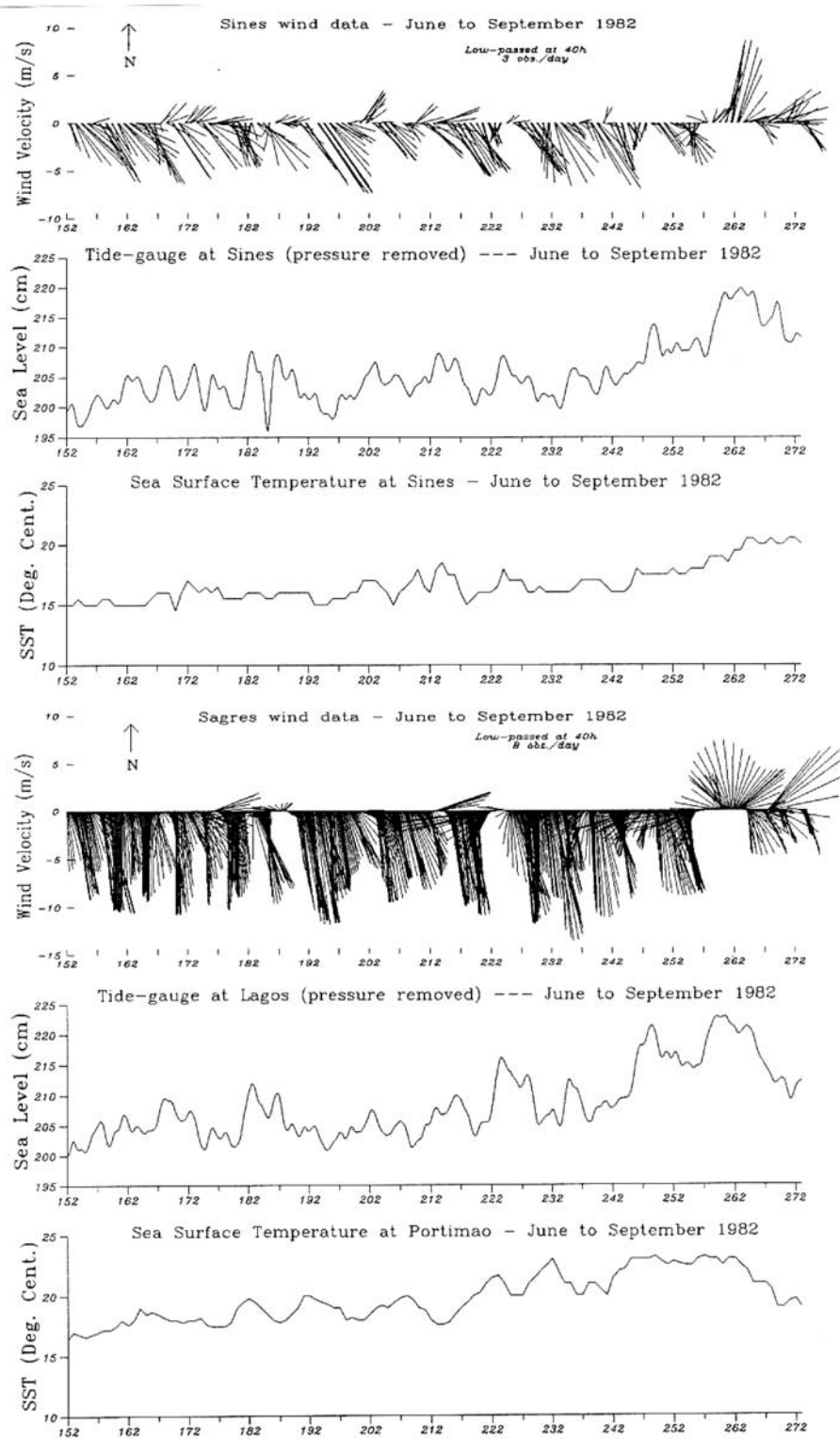
Figure 3. Evolution of coastal wind, sea level, and sea surface temperature compared to main features observed in the brightness temperature scenes of the Cape São Vicente region between June and September 1982. A rise in the symbols representing the features means its intensification. Information about the sampled AVHRR images is also displayed. A detailed description is given in the text.
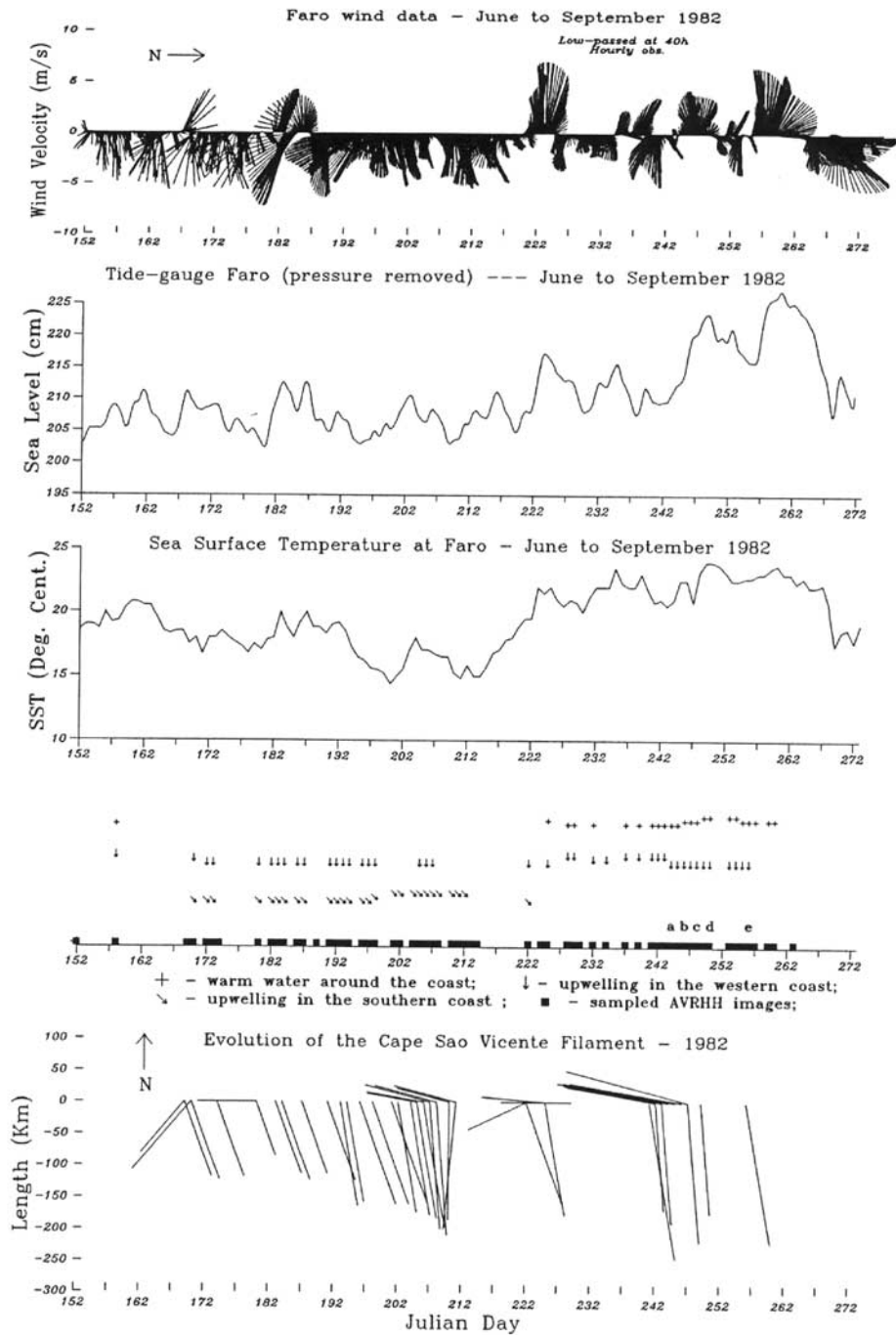
Figure 3. (continued)

summary of the evolution of the mesoscale features taken from the satellite images.

[19] The time series of the evolution of the orientation and length of the Cape São Vicente filament was taken from *Haynes* [1993]. He estimated these characteristics from the prints of AVHRR images to an accuracy better than ±20 km in the location of the offshore end of the filament and ±5° in the its orientation. The occurrence of upwelling in the western and south coast and the development of the coastal warm water band are also represented in Figure 3.

[20] Figure 3 shows that a persistent northerly wind was blowing along the west coast, with only weak and brief reversals, from the beginning of June till about 13 September (Julian day 257). Velocities over 5 m s^{-1} were common in Sines, the more northern site, but they frequently exceed 10 m s^{-1} in Sagres, near Cape São Vicente. The northerly wind at Sagres intensified as the season progressed, reaching its maximum velocity of 14.8 m s^{-1} about 20 September (day 233). In response, upwelling occurred on the western coast, and led to the growth and southward extension of the
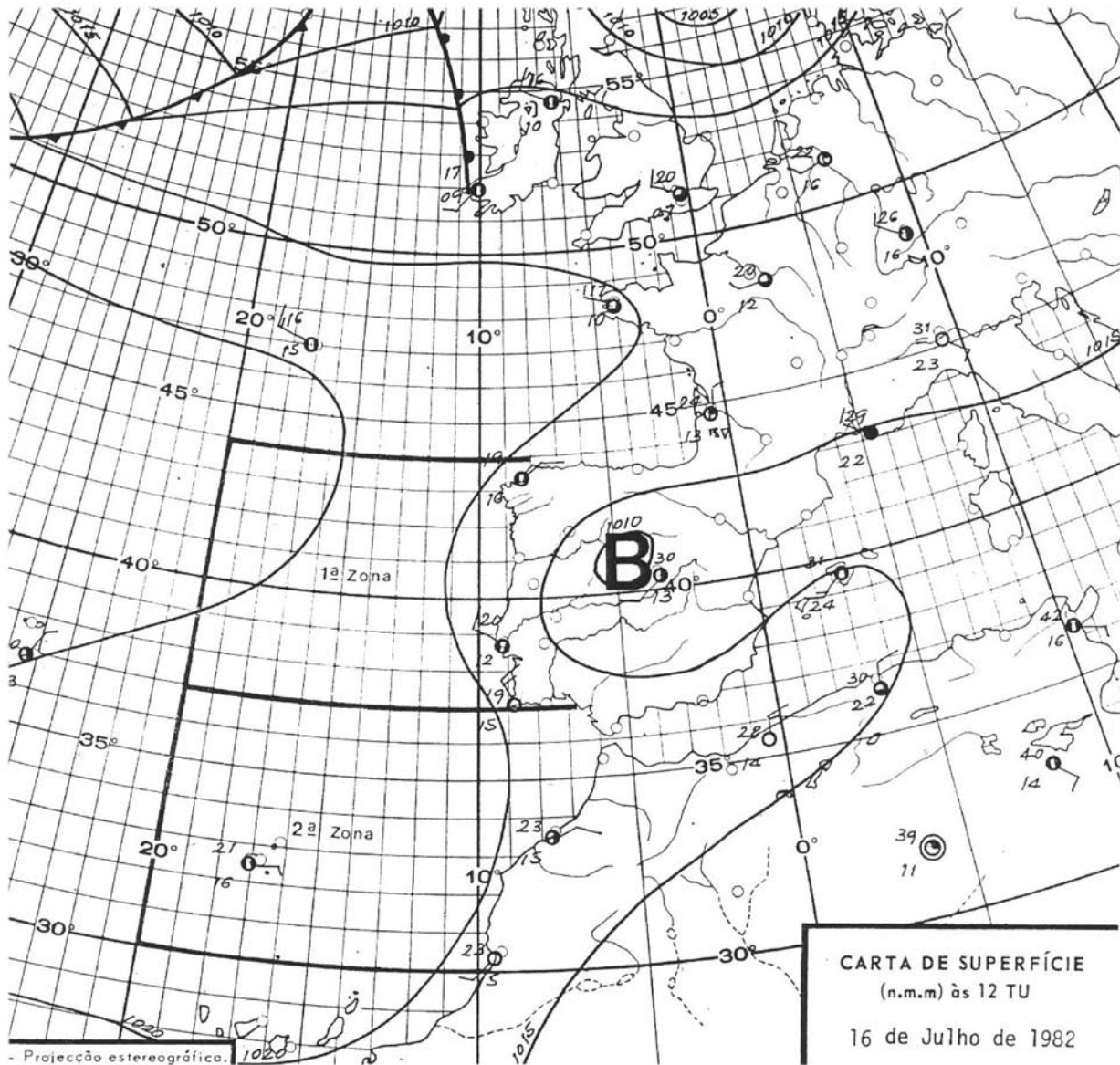
Figure 4. Surface meteorological chart of 16 July 1982 at 1200 LT showing a thermal low centered over the Iberian Peninsula, which corresponds to a typical summer pattern in this region.

Cape São Vicente filament. The maximum southward extent of the filament, about 250 km, occurred on 30 August (day 242), coincident with the final stage of a strong upwelling event off the west coast. This was the maximum length of the Cape São Vicente filament observed in the entire imagery archive. During this period a weaker westward branch of the filament also developed.

[21] In the south coast, at Faro, a more variable wind regime was observed (Figure 3). Typically, the summer wind pattern is affected by a thermal low over the Iberian Peninsula, forcing the northerly wind circulation along the west coast of Portugal to turn eastward at the latitude of the Algarve, as seen in the surface meteorological chart of 16 July 1982 (Figure 4). The orographic constraint of the ridge that extends zonally along the Algarve also helps rotate the

wind into a more east–west alignment. Following this general pattern, the wind was blowing eastward, upwelling favorable, till the beginning of August (about day 220), but was much weaker than on the west coast. In response, an upwelling regime was present, although two short relaxation events were observed about 16 June (day 167) and about 1 July (day 182). After the beginning of August, variable easterly winds were dominant till mid September (about day 262). By the end of the period, the wind had reversed to westerly again. Coincident with the occurrence of easterly winds, the upwelling regime ceased and the narrow band of warmer water started to develop from the east along the south coast.

[22] With the onset of the easterly winds the sea level in Faro rose significantly. The relative maximums were related
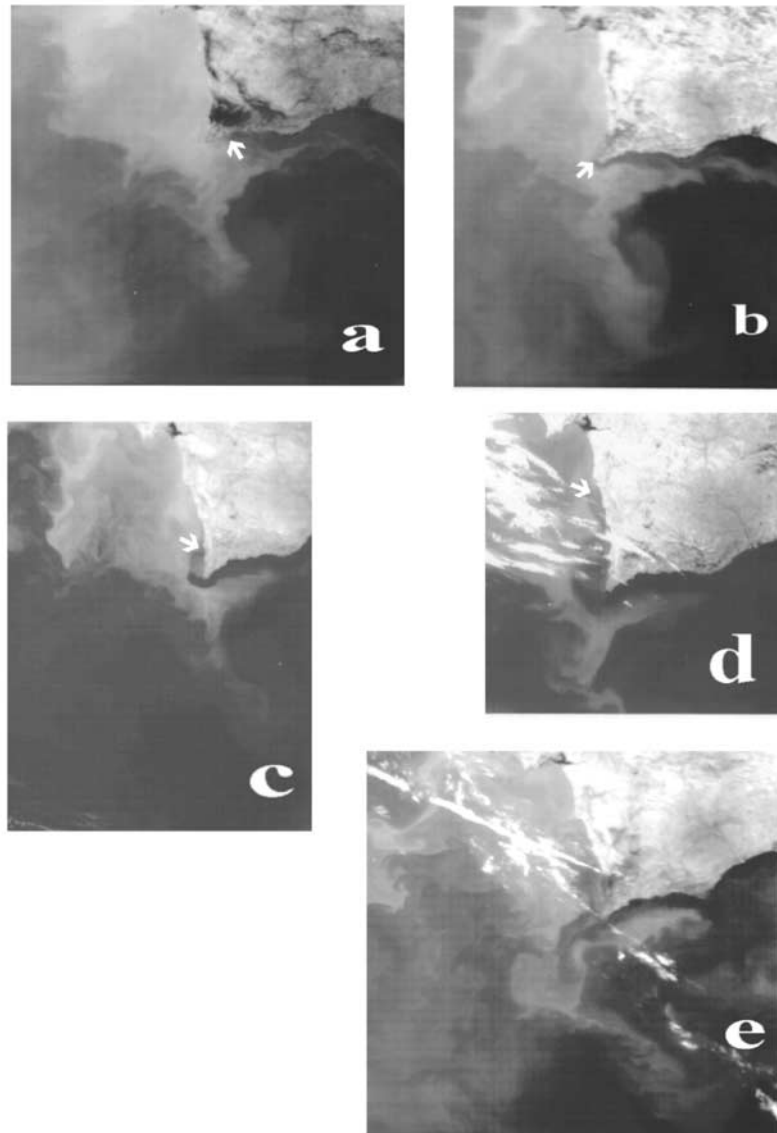
Figure 5. Raw AVHRR satellite images showing the westward progression and breakthrough of the coastal warm counterflow. Arrows point the leading edge of the warm counterflow. Images correspond to (a) 1 September at 0320 (day 244); (b) 3 September at 0256 (day 246); (c) 5 September at 0412 (day 248); (d) 7 September at 0337 (day 250); and (e) 13 September at 0417 (day 256), all from 1982.

to the stronger episodes of downwelling favorable winds. A similar behavior is also observed in Lagos, 72 km west of Faro. The lagged correlation between the two sea level time series gives a maximum of 0.90, significant at the 97.5% level, with Faro leading Lagos by 18 hours, meaning a progression of the signal of 96 km d^{-1}. In consecutive AVHRR images, the warm water band progressed along the south coast 31 km from day 244 (1 September) at 0320 till day 246 (3 September) at 0256 and 33 km from then till day 248 (5 September) at 0412, representing a steady flow with a speed of about 16 km d^{-1}. The monochrome AVHRR images are displayed in Figure 5. The timing of the images is shown in Figure 3. Arrows indicate the leading edge of the coastal warm water. Although there is some uncertainty in these estimates, because of the difficulty of tracking features from one image to the next, this evidence suggests that the rise in the sea level is primarily caused by the decline of the upwelling rather than by the progression of the warm water. With the end of the upwelling and the westward progression of the warm water, an increase in nearshore surface temperature of about 5°C in Faro and 3°C in Portimão is observed. Near the end of the time series, a drop in sea level and nearshore temperature occurred in response to the reestablishment of westerly wind and the related upwelling. However, no satellite images were available for that time.

[23] The coastal warm intrusion advanced about 60 km between day 248 (5 September) at 0412 and day 250 (7 September) at 0337 (Figures 5c and 5d), turning around Cape São Vicente and advanced northward along the west coast, at about 30 km d^{-1}, almost double the speed in the south coast. This occurred during a relaxation of the northerly wind at both Sines and Sagres. At that time, the

upwelling was limited to the part of the west coast north of 37.5°N, and the Cape São Vicente filament was separated from the cape by the warm flow, but continuous with water upwelled farther north. Subsequently, a short interlude of northerly wind intensification occurred and the warm water ceased its northward progression along the coast. Instead, it was diverted westward on 13 September (day 256) as an offshore prolongation of the flow along the south coast of Algarve (Figure 5e). The warmer water crossed the bathymetry into deep water by breaking through the filament, which became separated from the cool upwelled water off the west coast. Subsequently, the separated filament lost definition and began to decay. Also the cool water over the south coast continental slope became separated from the water upwelled on the western coast. Simultaneously, a pronounced relative minimum in the tide gauge records of Faro and Lagos, on the south coast, suggested the sudden release of the warm water accumulated in the south coastal region over the cooler denser offshore water. This pattern of warm water "breakthrough" occurred seven times during the 14 years covered by the satellite imagery archive.

[24] By mid-September (day 259), a wind reversal occurred at all three wind stations and southerly downwelling favorable winds of about 8 m s^{-1} were observed on the west coast. As upwelling ceased off the west coast, the warm intrusion developed northward as a coastal counterflow, reaching Sines by the end of the analyzed period. A rise in the sea level and a significant warming of the nearshore surface temperature then occurred at Sines, clearly out of phase with those in the southernmost stations.

[25] Similar analyses were made for the summers of 1985, 1990, and 1991, although the sets of observations were not so complete. The patterns were consistent with those of 1982.

5. Characteristic Sea Surface Temperature Patterns

[26] Individual and sequences of AVHRR images available in digital format were used to clarify and analyze the sea surface temperature patterns and their evolution. The aim is to illustrate and examine the typical patterns, rather than to study individual cases. Stick diagrams of the wind time series, or the mean wind vectors for the 72 hours prior to the image time are displayed, as detailed later. Images were processed for sea surface temperature as described above, and the 100, 200, and 500 m depth contours were overlaid.

5.1. Upwelling Patterns

[27] Upwelling occurred off the west coast all summer 1988 in response to prevailing northerly winds. On 25 July a wide band of cooler upwelled water was situated along the west coast (Figure 6). The thermal front between the upwelled water and the warmer offshore waters was contorted by small-scale disturbances. A major filament was present to the west, but with no evident relation with Cape São Vicente. The coastal southward jet associated with the upwelling regime appears to advect cool water along the shelf break eastward around Cape São Vicente. It is unlikely this frequently observed pattern could be generated by shelf edge upwelling, because of the weakness of the south coast winds.

[28] Upwelling persisted off the west coast till the end of August. The temperature anomaly with respect to offshore waters caused by upwelling was about 5°C but the thermal front was diffuse. A pronounced cold minimum was observed at Cape São Vicente, following the general pattern of enhanced upwelling in the vicinity of capes [e.g., *Kelley*, 1985; *Batteen et al.*, 1999], possibly forced by localized intensification of the wind or associated with flow separation and divergence. An ill defined filament extended westward from the cape and a weak upwelling occurred in the western part of the south coast. By the beginning of September a filament extended about 80 km southward from Cape São Vicente. Farther west offshore warm waters migrated poleward and the westward extending filament disappeared. However, by 5 September the upwelling in the west coast had abated with a wind relaxation, the equatorward filament had weakened, and the extent of cool water along the south coast had decreased. Scenes from 30 September and 1 October show a pattern similar to that from the end of July. The Cape São Vicente filament did not grow into a full developed structure during the upwelling season of 1988, although upwelling was present in the west coast during most of the season. In all the years covered by the imagery archive, this was the only one without a consistent development of the Cape São Vicente filament.

[29] The characteristic patterns of this filament are seen in sea surface temperature images of Figures 7, 8 and 9. Low-pass filtered wind vectors at Sines, Sagres and Faro are represented so that the ordinate represents the alongshore wind component, with negative values indicating an upwelling favorable wind component. Filament formation is always preceded by periods of west coast upwelling, driven by relatively intense alongshore northerly wind, and the filament persists until the wind weakens. For instance, in the sequence of thermal images of the first half of August 1991, shown in Figure 7, upwelling was established along the western coast during early August, in response to relatively intense southward wind, above 8 m s^{-1}. The Cape São Vicente filament developed with a surface thermal signature of about 3°C and grew southward, reaching a length of about 110 km by 2 August (day 214) and 160 km by 9 August (day 221). Similar wind patterns associated with the filament formation are seen in Figure 8 (26 August 1985, day 238, and 4 September 1985, day 247) and Figure 9 (16 September 1984, day 260).

[30] Coming back to Figure 7, upwelling was present along the south coast by 2 August (day 214), in response to a short westerly wind event (7–8 m s^{-1}) recorded at Faro. Upwelling later retreated along the south coast as a consequence of the relaxed winds recorded at Faro, and south coast warm water progressed westward, even turning clockwise around the cape by 13 August (day 225), profiting from easterly winds blowing at that time along the south coast. Also, in 4 September 1985 (day 247; Figure 8) and 16 September 1984 (day 260; Figure 9) upwelling is absent from the south coast and the coastal warm water band is seen to expand westward, despite some weak unfavorable westerly wind (<3 m s^{-1}), leaving cooler water offshore over the continental slope.

[31] In all the above situations, the southward filament was present at Cape São Vicente, showing a clear independence between upwelling on the southern coast and the
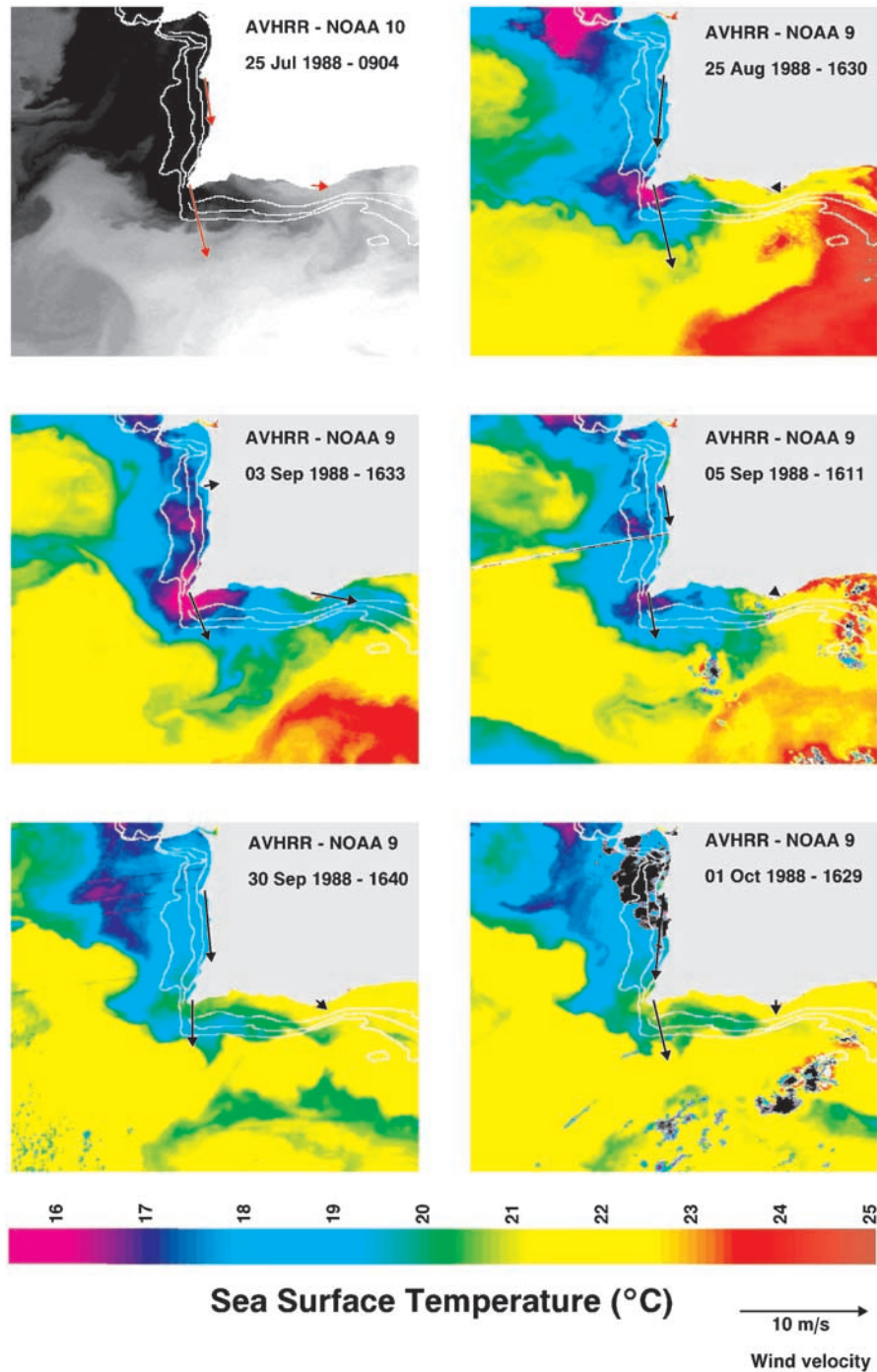
Figure 6. Thermal infrared NOAA-AVHRR images for the summer of 1988, when upwelling occurred off the west coast. The first image (NOAA 10) was processed only for brightness temperature. The other images (NOAA 9) were processed for sea surface temperature. The 100, 200, and 500 m depth contours are overlaid to the images. Wind vectors, computed as explained in the text, are plotted at Sines, Sagres, and Faro.

filament. This filament apparently constitutes the southward continuation of the equatorward coastal jet associated with the west coast upwelling overshooting the cape.

[32] In Figure 7, a second filament branch extends roughly westward from the cape. By 10 August (day 222) it has a length of about 130 km. Such westward filament structure is also observed in the satellite images in Figures 8 and 9. This formation might represent an offshore trending limb of a meander of the equatorward geostrophic flow associated with the upwelling. Another possible mechanism would be the presence of an eddy drawing cooler water offshore, although no clear evidence of such an eddy is seen in the
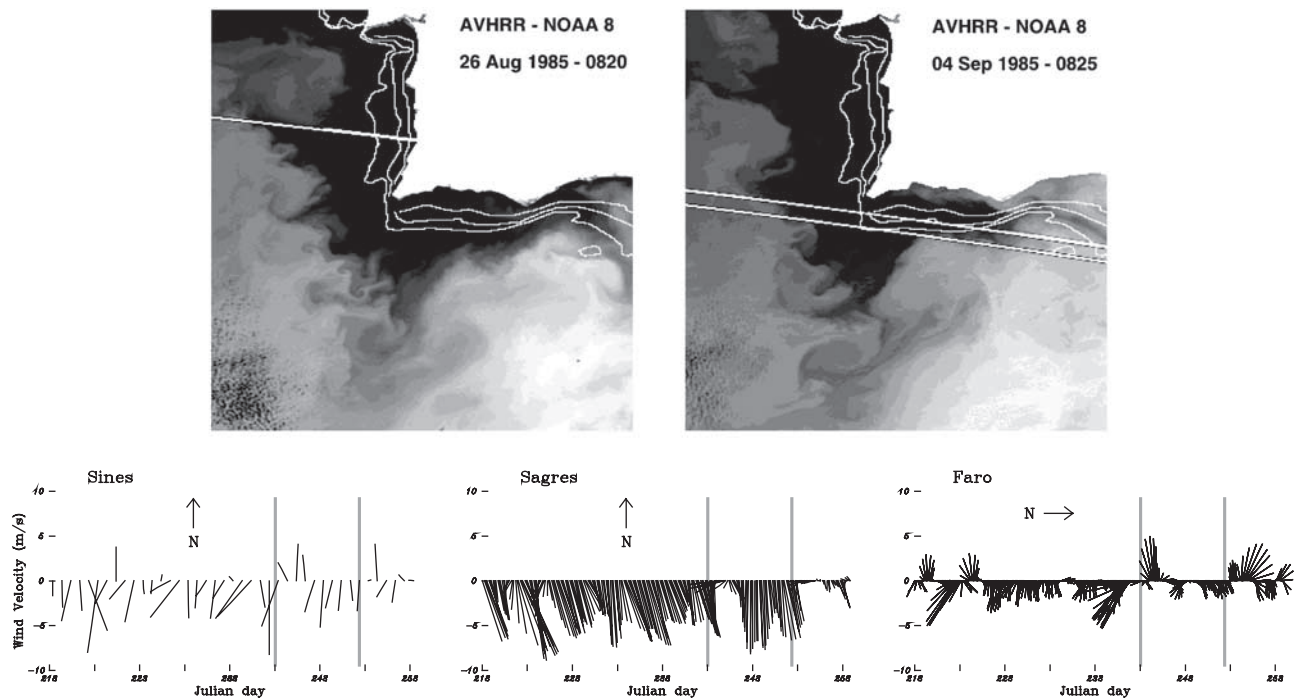
Figure 7. Set of thermal infrared NOAA-AVHRR images for the first half of August 1991, when the Cape São Vicente filament was developing. Images were processed for sea surface temperature. The 100, 200, and 500 m depth contours are overlaid to the images. Stick vector time series of the wind field measured at Sines, Sagres, and Faro from 15 July till 15 August are also displayed. Wind vector ordinate represents the alongshore wind component. Image dates are indicated in the stick diagrams (2 August, day 214; 9 August, day 221; 10 August, day 222; and 13 August, day 225).

sea surface temperature field. An onshore return flow located to the south of the filament jet, much weaker than the jet itself, seems to be a characteristic feature of the filament structures [*Strub et al.*, 1991; *Ramp et al.*, 1991]. Such return flow would partially feed the southward filament.

[33] The sea surface temperature field shown in Figures 7, 8, and 9 illustrates the pattern of the most developed upwelling in the Cape São Vicente region: two filaments extending equatorward and westward from the cape, and a

"tongue" stretching eastward along the southern continental shelf edge. These are particularly evident in the image of 16 September 1984 (Figure 9). The cool tongue is stable and persistent, sometimes narrow, having a length of 20–150 km, reaching occasionally as far as the Gulf of Cádiz. This cool water probably results from the topographic steering of coastal water along the depth contours around the Cape São Vicente. It often merges with waters upwelled off the Algarve, which were separated from the coast by the west-

Figure 8. Thermal infrared NOAA-AVHRR images of 26 August (day 238) and 4 September (day 247) 1985. Images were processed for brightness temperature. The 100, 200, and 500 m depth contours are overlaid to the images. Stick vectors time series of the wind field measured at Sines, Sagres, and Faro from 1 August till 10 September are also displayed, and the image dates are indicated. Wind vector ordinate represents the alongshore wind component.

ward progression of the warm coastal counterflow. The westward filament has a large variation in direction and development and occasionally rolls cyclonically in the offshore end. Sometimes it is ill defined or does not appear. The southward filament is frequent, well developed and varies appreciably in configuration but not in direction. Frequently it rolls cyclonically or grows into a vortex pair with an inverted mushroom-like shape.

[34] The possible role of Mediterranean outflow in distorting the surface patterns, especially the filament configuration, ought to be considered. After entering the Gulf of Cádiz at depths about 300 meters [*Ochoa and Bray*, 1991], the Mediterranean water splits into several cores flowing westward at different depths [*Zenk*, 1975; *Ambar and Howe*, 1979]. A shallow (400–600 m) core of Mediterranean outflow flows close to the Iberian Peninsula, continuing westward along the southern shelf break off Algarve [*Ambar*, 1983]. South and southwest of Cape São Vicente the Mediterranean water is observed to be present at 1000–1200, turning clockwise around the cape and being advected northward along the western Portuguese coast [*Meincke et al.*, 1975; *Zenk and Armi*, 1990; *Rhein and Hinrichsen*, 1993]. The spreading pattern of the Mediterranean water reveals the frequent existence of highly energetic eddies (meddies) at that level [*Richardson et al.*, 1991], while a shallower meddy at the secondary Mediterranean salinity maximum depth (700–800 m) is described by *Pingree and Cann* [1993]. The Cape São Vicente region is cited as a preferred region of meddies formation [*Armi and Zenk*, 1984; *Prater and Sanford*, 1994; *Bower et al.*, 1997; *Jungclaus and Mellor*, 2000], and there is some evidence

that the dynamic influence of meddies can extend to the surface [*Stammer et al.*, 1991; *Hinrichsen et al.*, 1993; *Pingree and Cann*, 1993]. The vertical coupling between meddies and surface features, yielding an indirect surface signature in temperature, salinity and potential density is reported by *Tychensky and Carton* [1998] in the Azores current region. The existence of a surface thermal signature of meddies would be expected were there a coupling between the surface and the mid-depth flow. Such conditions are more likely in the Iberian region in winter, when the poleward surface flow of warm waters of subtropical origin prevails. The near-surface nature of filament structures, and their dependence on vigorous coastal upwelling dynamics, indicates meddies are not a factor in the filament formation process per se. Nevertheless they could modify the form of developing filaments.

[35] During the upwelling season, the most persistent feature of the pattern is the cool eastward tongue stretching over the southern continental slope, followed by the southward filament and then by the westward filament. However, east, south, and west are the three preferred directions of development of the cool features. It is rare that a filament grows with a southwestern or southeastern direction.

[36] The frontal region that separates the cool filament waters from the surrounding warmer waters is almost always populated by conspicuous small-scale disturbances. Those are particularly evident in the filament presented in Figure 9, suggesting the instability of the southward jet inside the filament. Also in the satellite image of 26 August 1985 (Figure 8), a well-defined series of regularly spaced small perturbations oriented outwards is seen to contort the
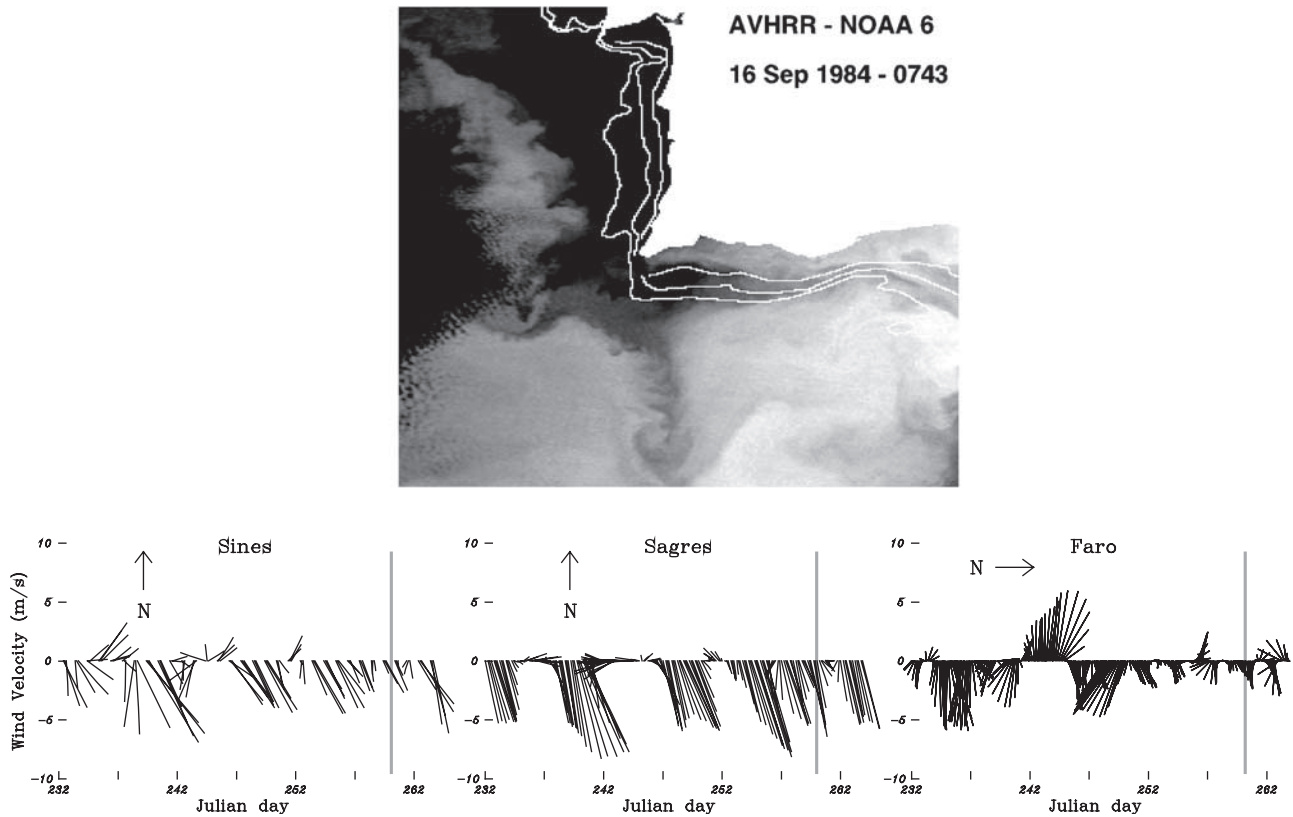
Figure 9. Thermal infrared NOAA-AVHRR image of 16 September (day 260) 1984. Image was processed for brightness temperature. The 100, 200, and 500 m depth contours are overlaid to the images. Stick vectors time series of the wind field measured at Sines, Sagres, and Faro from 20 August till 20 September are displayed, and the image date is indicated. Wind vector ordinate represents the alongshore wind component.

western boundary of the filament. These perturbations bend cyclonically at their outer limit, resembling small-scale replicas of filament features.

[37] Cloud-free images from late summer and early autumn of 1993 (Figure 10) show the upwelling response off the south coast of Algarve to westerly winds. As seen before, south coast upwelling is less frequent and weaker than in the west coast; a pattern like this was seldom observed in the 14 years archive of images (only six cases). Upwelling intensified during the second half of September, producing a strong temperature contrast with the offshore waters of about 5°C. The outer limit of the upwelled waters did not extend far beyond the continental slope, in contrast with the west coast. Off the west coast shelf and slope, a tongue of warmer water was apparently supplied from the warm water lying farther south off the Algarve coast. By the end of October the wind reversed at Faro and upwelling started to decay in the east. A generalized cooling of the surface waters occurred and a small cold plume grew westward from Cape São Vicente, as upwelling strengthened off the west coast.

5.2. Nonupwelling Patterns

[38] The nonupwelling pattern in the imagery corresponds always to the development of a warm water band along the coast. The extent of its development depends on the occurrence of west coast upwelling. A good example, showing the

progression and recession of this feature between 27 July and 12 August 1992 is presented in Figure 11.

[39] In the initial stage (27 July), upwelling was present off the west coast but not off the south coast, where the warm water band was developing nearshore under light easterly winds (<2 m s^{-1}). A zonal tongue of cool waters extended eastward along the shelf edge, apparently the continuation around Cape São Vicente of the equatorward coastal current. By 4 August the narrow warm band was clearly defined, with a temperature signal of about 3.5°C. As the upwelling regime relaxed on the west coast, the leading edge of the coastal warm intrusion turned around Cape São Vicente, progressing about 110 km in 8 days ($\approx$14 km d^{-1}).

[40] The full development of the warm flow was reached on 8–9 August, when it passed Cape Sines. Although this feature appeared along the south coast whenever upwelling was absent, its extension along the west coast was more sporadic because of the higher persistence of upwelling there (only in 20% of the times it turns the cape to the west coast). From 4 August at 0454 till 8 August at 1530 the warm water advanced along the west coast by about 125 km ($\approx$28 km d^{-1}). The coastal warm water was confined to the continental shelf, had a width of 15–25 km, decreasing northward, and produced significant warming nearshore. Cooler water remained over the continental slope while farther offshore warmer waters migrated westward off the south coast then northward off the west coast. By 11–12
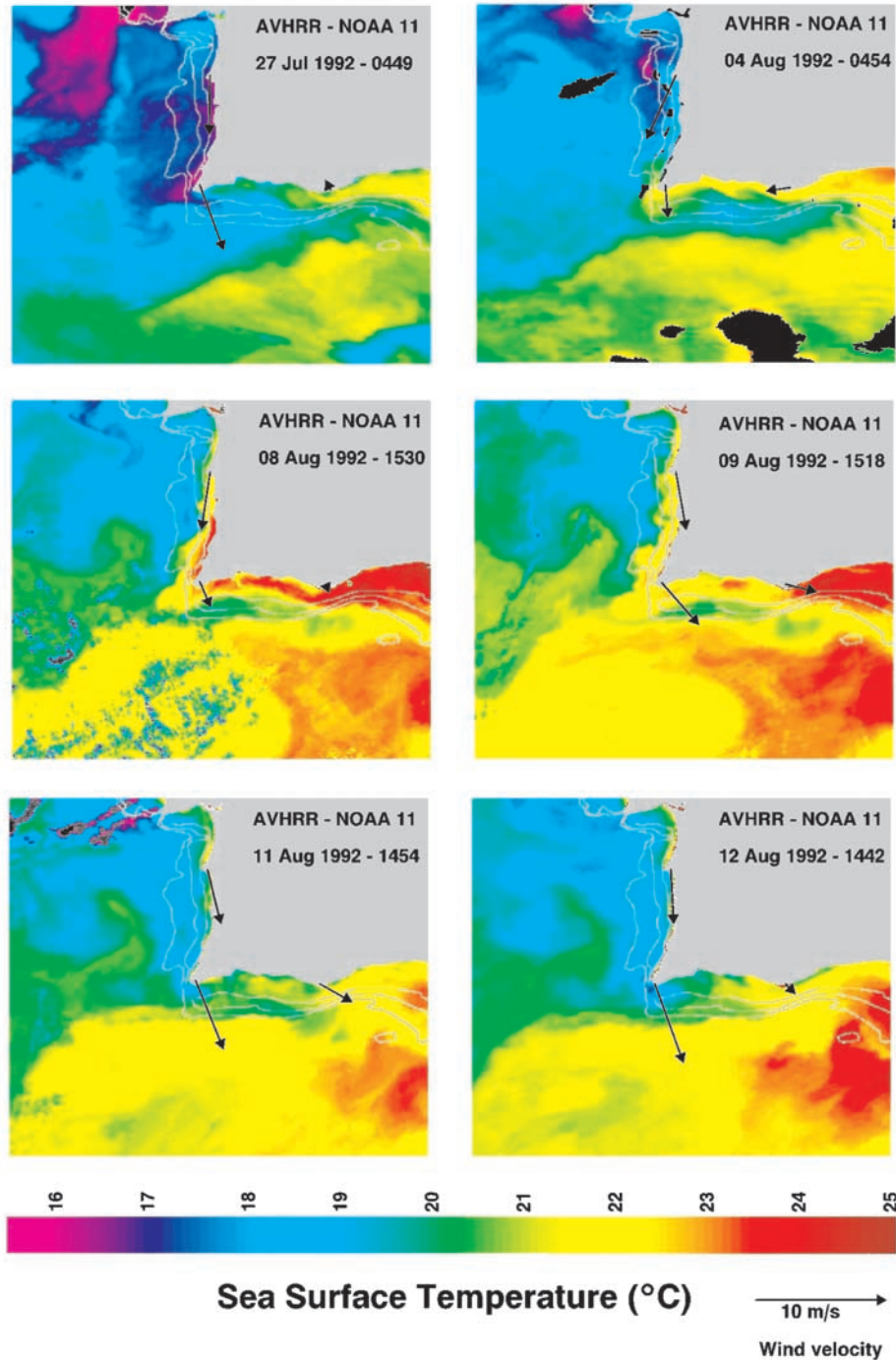
Sea Surface Temperature (°C)

10 m/s

Wind velocity
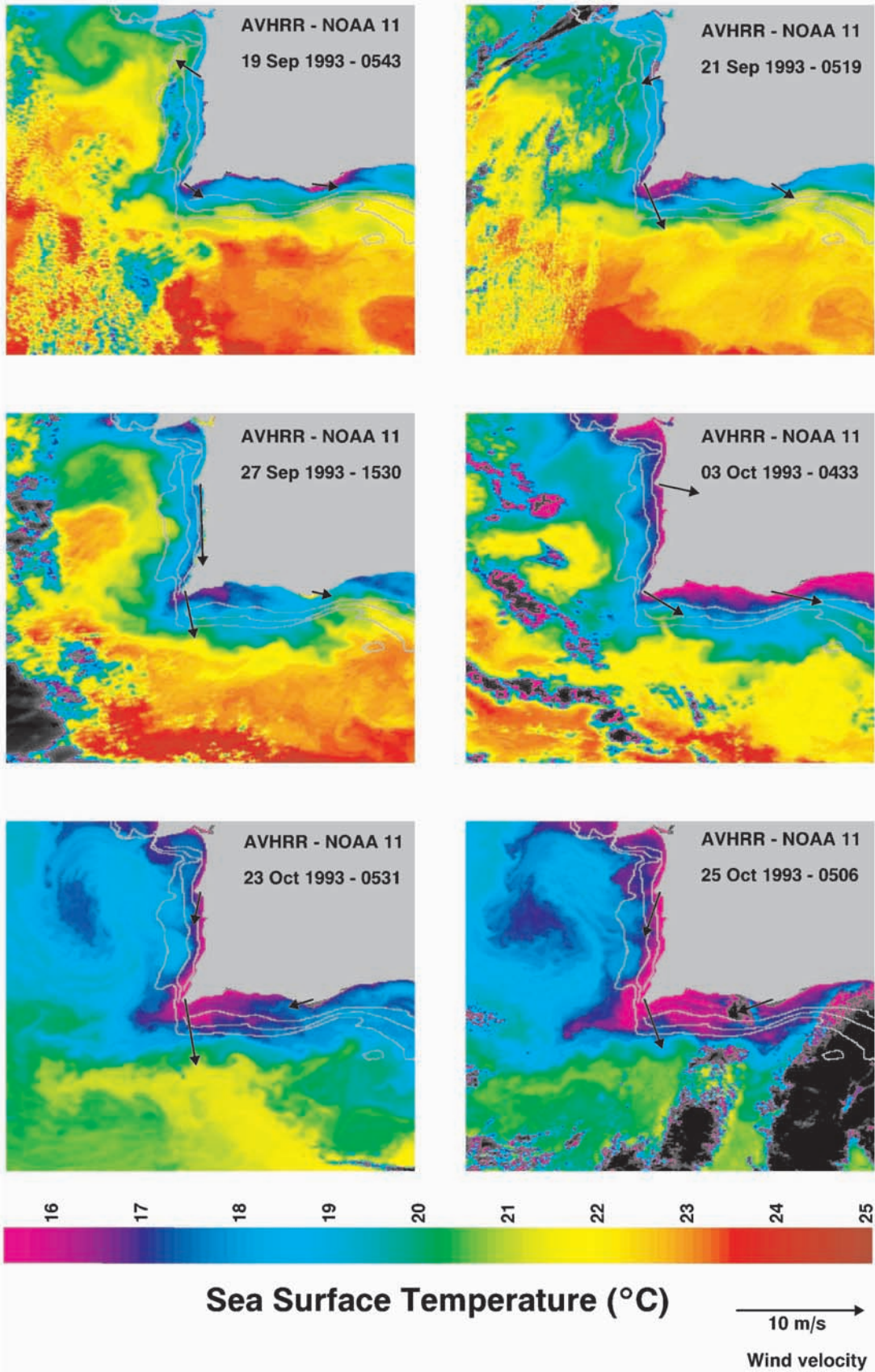
Figure 11. Set of thermal infrared NOAA-AVHRR images for the summer of 1992 showing the progression and retraction of a warm intrusion close to the coast in the Cape São Vicente region. Images were processed for sea surface temperature. The 100, 200, and 500 m depth contours are overlaid to the images. Wind vectors, computed as explained in the text, are plotted at Sines, Sagres, and Faro.

August the coastal warm feature had disappeared with the reestablishment of stronger winds and upwelling in the west coast, and colder water once again turned cyclonically, close to shore, around Cape São Vicente. Off the south coast

winds reversed to westerly and the warm feature started to retreat eastward.

[41] The alongshore advance of the warm water was at speeds remarkably similar to those estimated earlier for the

Figure 10. (opposite) Set of thermal infrared NOAA-AVHRR images showing an upwelling episode in the south coast of Algarve. Images were processed for sea surface temperature. The 100, 200, and 500 m depth contours are overlaid to the images. Wind vectors, computed as explained in the text, are plotted at Sines, Sagres, and Faro.

Table 1. Progression Speed of the Coastal Warm Counterflow off the South and West Coast of Portugal, Estimated From AVHRR Images in Different Events

Year	Time Interval	South Coast Progression (Speed)	West Coast Progression (Speed)
1982	1 Sept. 0320–3 Sept. 0256	31 km (15.5 km d^{-1}; 18.1 cm s^{-1})	
1982	3 Sept. 0256–5 Sept. 0412	33 km (16.1 km d^{-1}; 18.6 cm s^{-1})	
1982	5 Sept. 0412–7 Sept. 0337		60 km (30.3 km d^{-1}; 35.1 cm s^{-1})
1986	19 July 0359–20 July 0348	14 km (14.1 km d^{-1}; 16.3 cm s^{-1})	
1988	18 Sept. 0104–19 Sept. 0524		39 km (33.0 km d^{-1}; −38.2 cm s^{-1})
1991	11 Aug. 0322–13 Aug. 0303	32 km (16.1 km d^{-1}; 18.6 cm s^{-1})	
1992	27 July 0449–4 Aug. 0454	110 km (13.7 km d^{-1}; 15.9 cm s^{-1})	
1992	4 Aug. 0454–8 Aug. 1530		125 km (28.2 km d^{-1}; 32.6 cm s^{-1})

summer of 1982 and for other years, as shown in Table 1. Accepting the surface temperature as an approximate tracer of the flow path, it is possible to presume that the non-upwelling pattern in the Cape São Vicente region is dominated by a warm coastal countercurrent, flowing with surface speeds of about $16-19$ cm s^{-1} westward along the south coast and $32-38$ cm s^{-1} poleward along the west coast.

[42] An explicit example of the coastal warm feature turning clockwise around the Cape São Vicente is shown (Figure 12) for 20 July 1986 (Julian day 202) with low-passed wind vectors at Sines, Sagres and Faro for July 1986. Sagres wind is shown twice, unrotated and rotated to the east–west direction, as was done with the Faro data. The "nose" of the warm feature is narrow but well defined, with a width about 10 km and a surface thermal signature of about 2°C. The pattern in the satellite scene corresponds to the end of a short period of weak south coast downwelling favorable winds (about 3 m s^{-1} at Faro and 2 m s^{-1} at Sagres). The warm feature turns poleward around the cape crossing the bathymetry and leaving some cooler water inshore. This occurred during a relaxation of the northerly winds at Sagres and Sines. Farther north along the west coast upwelling was still present, as was the usual pattern of cool water along the south coast continental slope.

[43] A different pattern observed at times when upwelling is absent from the south coast and the warm coastal countercurrent is setup, is exemplified by the AVHRR image of 19 September 1988 (Figure 13). Part of the warmer water flows poleward along the west coast, but the main part of the coastal warm water continues directly west from Cape São Vicente. It breaks through the body of cooler water that was previously established off the west coast and along the shelf edge and slope east of the cape. The warm lighter water crosses over the denser colder water and connects with the offshore warm water, apparently because of a weakening of the cooler equatorward jet or to the excess of water of the coastal warm counterflow. Cooler water stays isolated over the southern continental slope. This pattern is the same as that shown in Figure 5e.

6. Sea Level

[44] After removing tidal and other near diurnal effects from the sea level data and correcting the data for the inverted barometer effect, monthly mean six hourly sea level values were computed for Sines, Lagos, and V.R.S. António. The annual cycle of the sea level height at each location is shown in Figure 14. The V.R.S. António tide gauge is located close to the mouth of the river Guadiana, but this does not seem to affect the long term sea level height. The river has several dams and the outflow is generally weak year around. Any occasional rise of the outflow, due to any dam discharge or heavy rain has a timescale that would have been removed by the low-pass filter. A common pattern is observed at the three tide gauges, with minimum spatial variations. Monthly mean sea level increases toward the end of the year, and then drops to its lowest values in spring, in close agreement with the sea level annual cycle of the eastern North Atlantic.

[45] The monthly mean sea level height at the three tide gauge was compared with the dynamic height relative to 500 dbar calculated from the historical NODC hydrographic data. The reference surface of 500 dbar was chosen because of the paucity of data below this level. However, in coastal transition regions the physical processes reflected in seasonal pattern changes occur in general above 500 dbar. Below this level the density changes are negligible compared with those above. In the absence of knowledge of the variation in density associated with seasonal change in the Mediterranean outflow, it is assumed deep changes are small though this may be a source of error. The monthly mean dynamic height relative to the 500 dbar level was computed in the nodes of a grid of 50 km × 50 km from the historical profiles of temperature and salinity, previously binned in 13 levels between the surface and 500 m depth and gridded at each level by an objective analysis scheme [*Relvas*, 1999], using the standard algorithms recommended by *UNESCO* [1991]. Monthly mean sea level data of each individual tide gauge, adjusted for the inverted barometer effect, along with error bars for the standard deviation, are plotted in Figure 15 superimposed on the mean monthly dynamic height computed at the nearest node of the 50 km × 50 km grid. Location of the grid nodes used are also displayed. Given the different nature and the slightly different location of the data series compared, only the general features of the seasonal variation should be considered significant. The dynamic height data series agree well with the measured sea surface elevation data series in all three stations. Generally, dynamic height values fall inside the monthly standard deviation of the sea level height, supporting the validity of the 500 dbar reference level. The relatively good agreement between the seasonal variation of the measured sea level at V.R.S. António and the dynamic height pattern farther offshore at the closest grid node confirms the negligible influence of the river Guadiana outflow.

[46] Accepting the leveling of the tide gauges, realistic comparison of absolute sea level height at the different tide gauges stations is possible. The most important feature apparent in Figure 14 is the indicated alongshore coastal elevation slope, with sea level rising from Sines toward
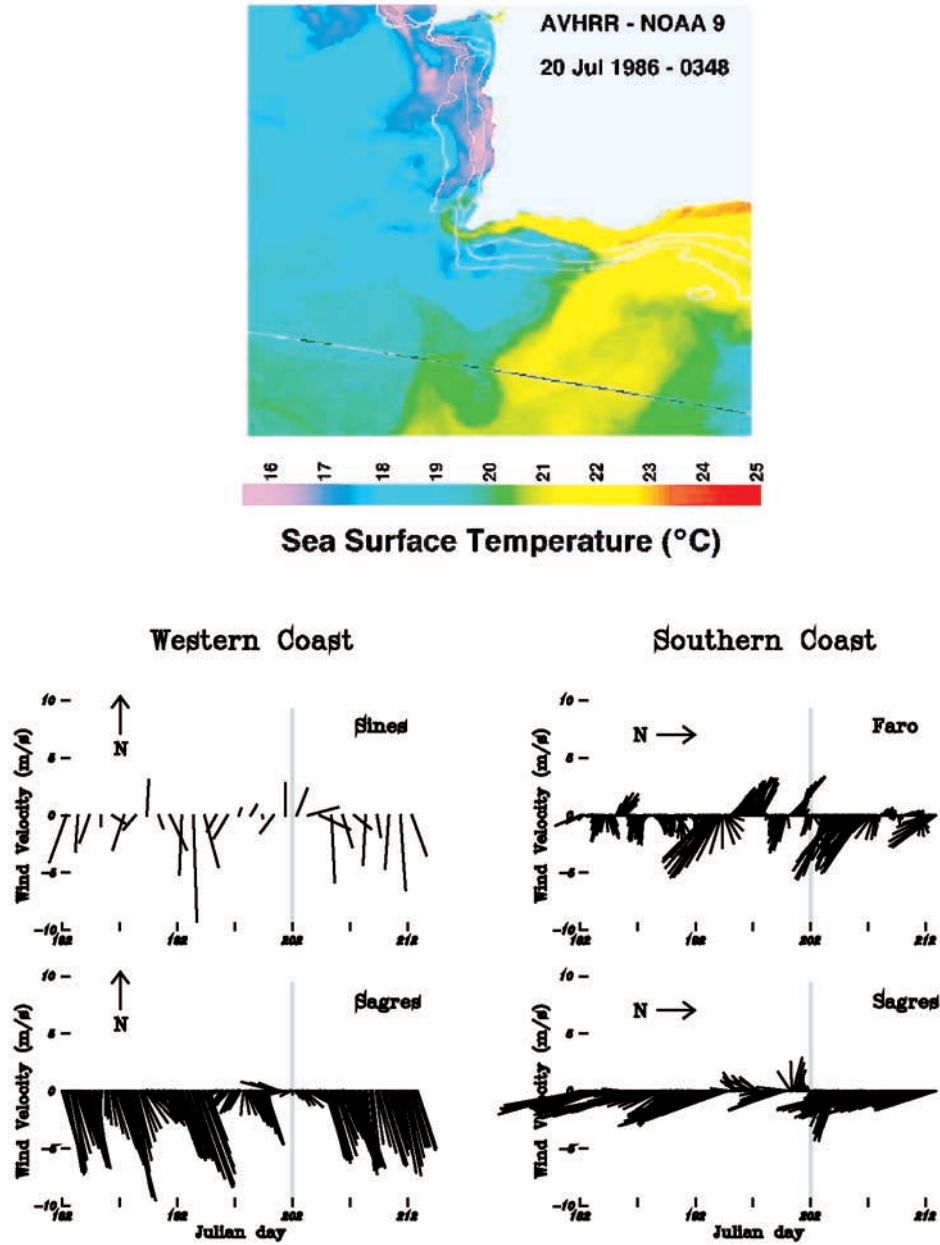
Figure 12. Thermal infrared NOAA-AVHRR image of 20 July 1986 (Julian day 202) showing the development of the coastal warm feature the Cape São Vicente region and the wind vectors (low-pass filtered at 40 hours) for July 1986 at Sines, Sagres, and Faro, rotated alongshore for the western and south coasts. Image date is marked in the stick diagrams. Image was processed for sea surface temperature. The 100, 200, and 500 m depth contours are overlaid to the image.

Lagos along the west coast, and from Lagos toward V.R.S. António, along the south coast. This pattern occurs throughout most of the year, with slight exceptions in November and December. Alongshore sea level slope is stronger in summer, with maximum values of 3.93×10^{-7} between Sines and Lagos (142.5 km distance) and 5.00×10^{-7} between Lagos and V.R.S. António (120 km distance) in August.

[47] The absolute alongshore pressure gradient is important to the circulation dynamics of the coastal region. The total pressure gradient consists of a barotropic and a baroclinic contribution. For a coastline parallel to the x axis, the total alongshore pressure gradient at a depth D (positive z upward) is given by *Chelton* [1984]:

$$\frac{\partial p}{\partial x} = \rho_0 g \frac{\partial \eta}{\partial x} + g \int_D^0 \frac{\partial \rho}{\partial x} dz \qquad (1)$$

where p is the pressure, g the gravitational acceleration, η the sea surface elevation, ρ the water density, and ρ_0 the surface water density. For shallow waters over the continental shelf, D is small, and if it is assumed that the vertically integrated alongshore density gradient is small, the barotropic mode is dominant and the pressure
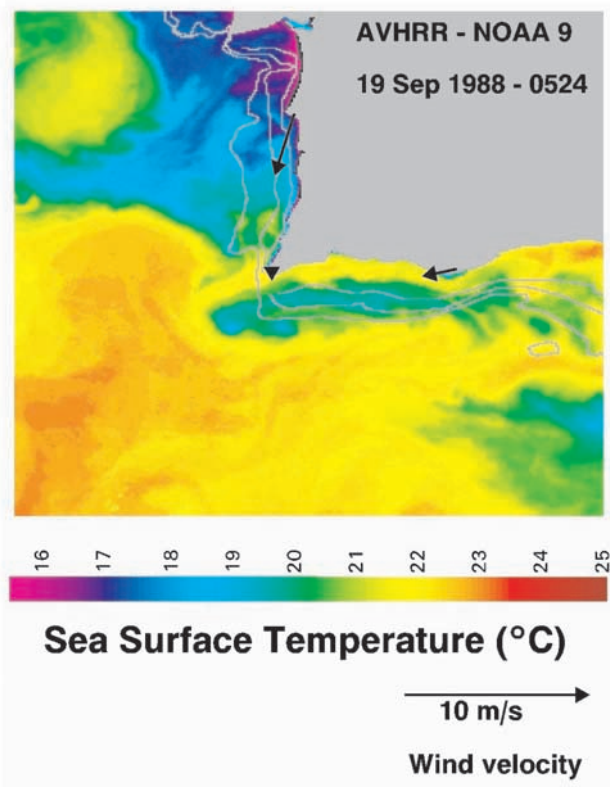
Figure 13. Thermal infrared NOAA-AVHRR image of 19 September 1988 showing the offshore release of the warm coastal feature near the Cape São Vicente. Image was processed for sea surface temperature. The 100, 200, and 500 m depth contours are overlaid to the image. Wind vectors, computed as explained in the text, are plotted at Sines, Sagres and Faro.

gradient is proportional to the surface sea level slope. The presence of any baroclinic component due to alongshore density gradient will tend to compensate the surface flow with depth.

[48] An independent check on the tide gauge leveling can be done by comparing the mean annual slope from the tide gauges with that from the dynamic height relative to 500 dbar (Figure 16). Mean annual dynamic heights were computed as above at the grid nodes closest to shore, but

off the shelf. The slope of the dynamic height has three sources of errors: sparse sampling may affect the result at any node; the choice of 500 dbar as the reference level near the slope, where a shallow Mediterranean water vein occurs [*Ambar*, 1983] may not be completely correct; and the assumption that the sea level slope is the same offshore and at the coast may not hold. However, the slopes estimated from the dynamic height and from the tide gauges have the same sense and order of magnitude.

[49] Thus, it seems evident that an alongshore monthly mean pressure gradient force acts during most of the year, favoring a coastal circulation westward along the south coast and northward along the west coast of southwestern Iberia. The strongest pressure gradient occurs in summer, when it is opposed by intense upwelling favorable winds, and the forcing is small or vanishes in winter.

7. Momentum Analysis

[50] For a coastline parallel to the x axis, the vertically averaged alongshore component of the linear momentum equation for a barotropic ocean can be written as [*Gill*, 1982]:

$$\frac{\partial u}{\partial t} = -fv - g\frac{\partial \eta}{\partial x} + \frac{\sigma_s}{\rho H} + \frac{\sigma_b}{\rho H} \qquad (2)$$

where u and v denote the vertically averaged alongshore and cross-shore components of velocity, respectively, f denotes the Coriolis parameter, σ_s and σ_b denote the surface stress imposed by the wind and the bottom stress due to friction, respectively, and H denotes the water depth.

[51] Accepting the geodetic levelling of the tide gauges, from July till September, mean sea level rises by 4.5 cm from Sines to Lagos along the west coast (142.5 km distance), and rises by 5.7 cm from Lagos to V.R.S. António along the south coast (120 km distance). The alongshore barotropic acceleration forced by the alongshore pressure gradient, if acting alone, is given by

$$\frac{\partial u}{\partial t} = -g\frac{\partial \eta}{\partial x} \qquad (3)$$

[52] For the observed alongshore pressure gradients, the barotropic acceleration is about 0.26 m s^{-1} d^{-1} between
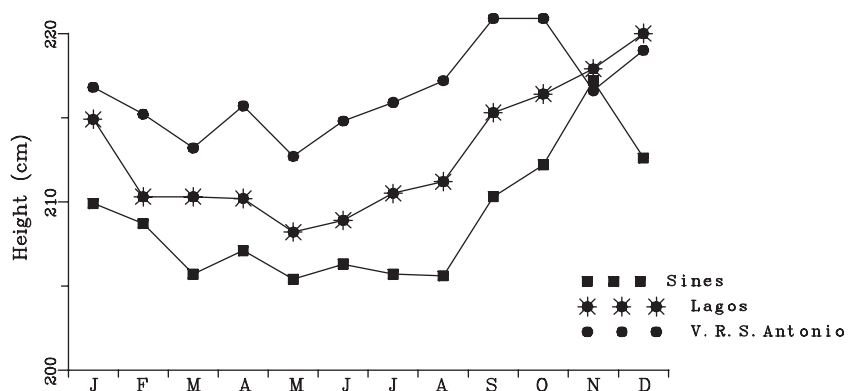

Figure 14. Mean sea level computed from tide gauge measurements, corrected for the inverted barometric effect at Sines, Lagos, and V.R.S. António.
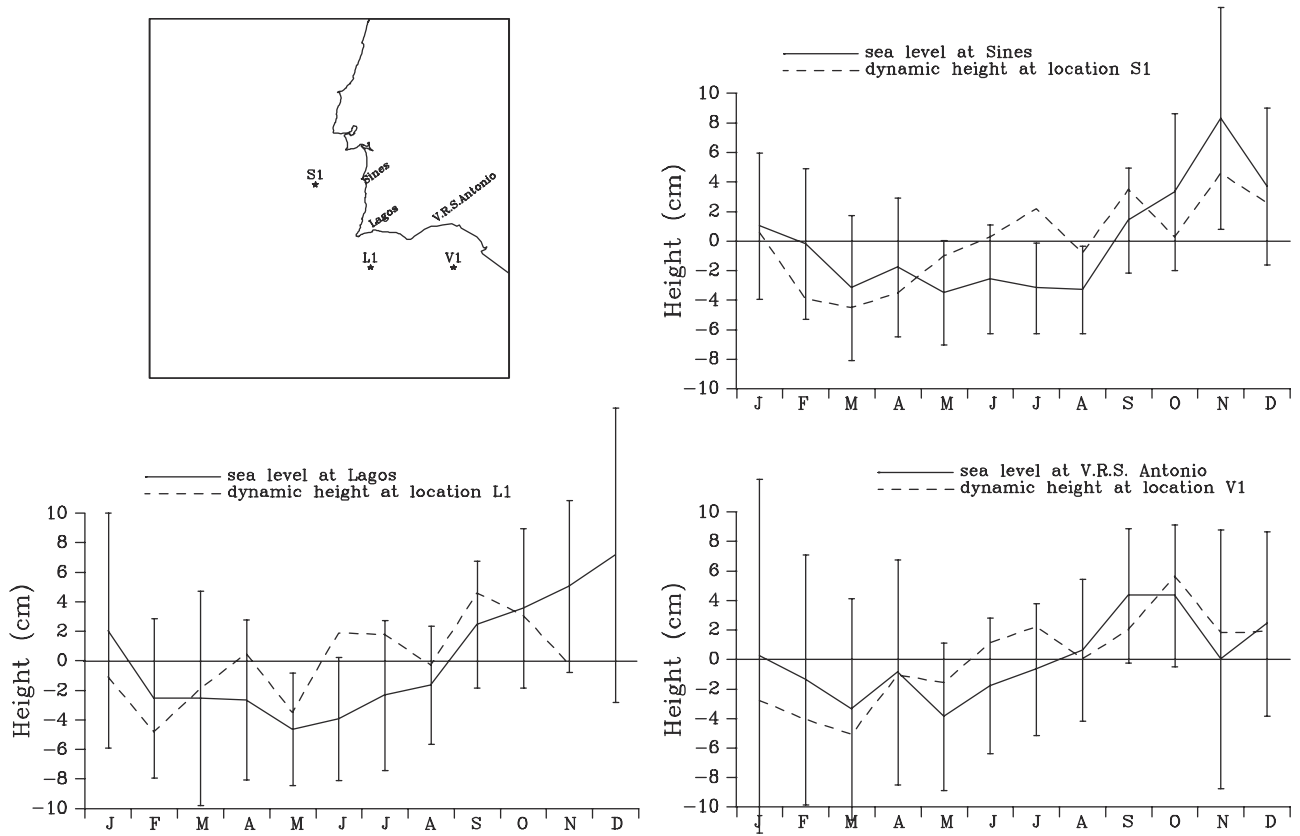
Figure 15. Dynamic height ($\Delta D_{0/500}/g$) (dashed lines) and sea level monthly mean seasonal variation (solid lines). Error bars represent the monthly standard deviations of the sea level. Dynamic height and sea level values were demeaned. Location of the tide gauges and position of the compared grid nodes are also displayed.

Lagos and Sines, along the western coast, and about 0.40 m s^{-1} d^{-1} between V.R.S. António and Lagos, along the south coast. So, the observed speed of advance of the warm coastal countercurrent could be reached in about one day, ignoring other factors. However, other effects retard the acceleration, in particular friction. Assuming now that a steady state is reached when the bottom stress equals the

alongshore pressure gradient, the balance equation can be written as

$$g\frac{\partial \eta}{\partial x} = \frac{C_b}{H}|\vec{V}_w|u_w \qquad (4)$$

with the bottom stress written as a quadratic stress law $\sigma_b = \rho C_b|\vec{V}_w|u_w$ [*Gill*, 1982], where $\vec{V}_w = (u_w, v_w)$ repre-
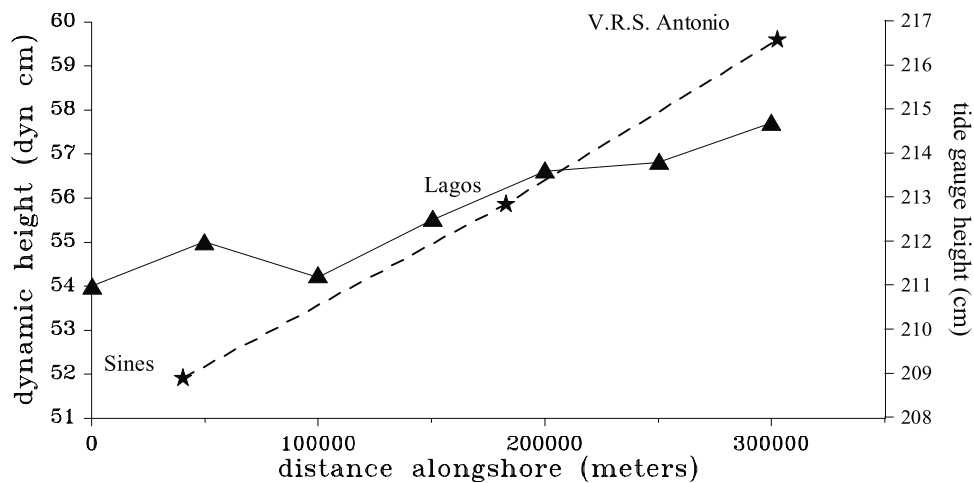

Figure 16. Alongshore mean annual slope from the tide gauges (dashed line) and alongshore dynamic height slope relatively to 500 dbar (solid line).

sents the near-bottom current vector, and C_b the bottom drag coefficient. Taking $C_b = 3.0 \times 10^{-3}$ [*Wang*, 1993] and considering the water depth of 100 m over the continental shelf, an equilibrium velocity of about 0.32 m s^{-1} is obtained for the west coast, and of about 0.39 m s^{-1} for the south coast. These values represent upper limits for the alongshore current velocities, when no surface friction is acting.

[53] However, the important role of surface wind stress was not considered here. As noted before, upwelling favorable winds blow during summer along both coasts, opposing the alongshore pressure gradient and slowing down the alongshore current. The estimates computed here suggest a quick response of the coastal ocean to the wind relaxation events, indicating a strong short scale variability of the alongshore current field.

[54] Recalling equation 2, it can be expected that the vertically averaged Coriolis term is small, because the depth average cross shelf flow is close to zero. The bottom stress will act to reduce any flow and when the current due to the alongshore pressure gradient is exactly balanced by an opposing wind stress, the bottom friction is zero. In this case, for a steady state flow, the vertically averaged alongshore flow is determined principally by the relative magnitude of the wind stress and the vertically integrated pressure gradient force for a given water depth, and so the balance equation 2 is reduced to

$$g\frac{\partial \eta}{\partial x} = \frac{\rho_a C_s}{\rho H}|\vec{V}_a|u_a \qquad (5)$$

with the wind stress written in its explicit form, $\sigma_s = \rho_a C_s |\vec{V}_a|u_a$, where ρ_a represents the air density, $\vec{V}_a = (u_a, v_a)$ represents the wind vector, and C_s the surface wind stress drag coefficient.

[55] The local alongshore wind stress and the alongshore pressure gradient force act in opposite directions. Simple calculations of equation 5, with $\rho_a = 1.225$ Kg m^{-3}, $\rho = 1027$ Kg m^{-3}, $C_s = 1.2 \times 10^{-3}$, and assuming a water depth of 100 m over the continental shelf, will imply a northerly alongshore wind velocity of 14.5 m s^{-1} in order to balance a mean sea level slope of 4.5 cm between Sines and Lagos, and a westerly alongshore wind velocity of 17.8 m s^{-1} in order to balance the mean sea level slope of 5.7 cm between Lagos and V.R.S. António. Thus, in mean terms, the alongshore pressure gradient forces a vertically averaged alongshore flow, westward along the south coast and northward along the west coast, unless the wind velocity exceeds the above values and forces the alongshore flow to reverse.

[56] On a long timescale such alongshore wind velocities are unlikely to occur (15 m s^{-1} is exceeded only in 1% of west coast wind observations). However, previous works report a southward coastal current over the shelf and continental slope off the west coast of Portugal during summer [*Fiúza*, 1983, 1984]. No direct measurements of currents off the south coast have been made. A source of subjectivity on the computation of a wind threshold to reverse the direction of the coastal flow is the assumed value of the water depth, H. This applies strictly to a well mixed coastal ocean, in which all the water column is dragged by the wind stress. However, in a stratified ocean

the wind stress acts only in the layer above the pycnocline, and so the effective value of H can be much less that the bottom depth.

[57] Observations carried out in the region during the early summer [*Relvas and Barton*, 1995] revealed the existence of a pycnocline in the region, with a mean depth about 30 meters. Analysis of the vertical distribution of the density field based on the historical NODC data (not shown here) also suggests the existence of a summer pycnocline at that depth. Assuming a stratified ocean and taking H = 30 m, equation 5 indicates alongshore wind velocities above about 7.9 m s^{-1} and 9.7 m s^{-1} will reverse the near-surface flow off the western and south coasts respectively. This formulation implies the presence of vertical shear in the water velocity. Such alongshore wind velocities seem more realistic since they are more likely to occur and persist during longer time periods, in view of the observed wind variations. Winds above 8 m s^{-1} account for about 15% of the observations at Sagres.

[58] Assumptions made here are somewhat subjective. Apart from uncertainties in, for example, thickness of the mixed layer and surface drag coefficient, a major possible source of error lies in the leveling of the tide gauges, although an accuracy of 0.5 cm is stated by Instituto Hidrografico. However, the agreement within a factor of two with the estimated dynamic height slope is encouraging, and the results are strongly supported by remote sensing. The goal was to demonstrate that the wind-forcing, under certain conditions, could drive the coastal flow against the alongshore pressure gradient. Conditions of upwelling favorable wind are characteristics of the summer on both coasts, but the threshold necessary to drive the equatorward coastal flow is more easily reached on the west coast, because of the weaker alongshore pressure gradient and stronger winds in summer there. The response of the coastal ocean to the wind relaxations, reestablishing the alongshore flow, is of the order of 2–3 days.

8. Discussion

[59] The presence of a meridional pressure gradient off western Iberia all year, balanced during the summer by the southward wind stress, was hypothesized earlier by *Frouin et al.* [1990]. However, no driving mechanism has been suggested for the southern (zonal) coast of Iberia. Based on satellite imagery and large-scale meteorological considerations, *Fiúza* [1983] concluded that without westerly winds, the coastal circulation off southern Portugal seems to be predominantly westward. Evidence from cruise observations carried out by *Haynes and Barton* [1990] during September 1986 off western Iberia in a situation of post-upwelling, showed a poleward flow on the continental shelf, associated with the northward advection of anomalously warm and salty water with water mass characteristics similar to waters from the Gulf of Cádiz. This suggests a continuity of the flow along the south coast of Iberia, and northward around Cape São Vicente. The magnitude of the sea surface tilt, which is strong when compared with sea surface slopes off California [e.g., *Ramp and Abbott*, 1998], suggests that the pressure gradient force may be of primary importance to the generation of the counterflow, although during winter its influence is reduced. During the summer, this flow is

overcome off the west coast, at least in the upper layers, by the equatorward geostrophic current resulting from local upwelling forced by the northerly winds. Off the south coast such a situation occurs only occasionally during the summer, because strong upwelling favorable winds are less common. The differences in wind forcing between the west and south coasts provoke conspicuous phenomena in the Cape São Vicente region when the southward current off the west coast encounters the westward flow along the south coast, as observed in the satellite imagery.

[60] The origin of the alongshore pressure gradient is not precisely determined. In regions where the shelf is narrow, deep ocean currents may affect the alongshore elevation slope [*Hickey and Pola*, 1983]. A core of the Mediterranean outflow with an equilibrium depth between 400 and 700 m flows westward along the southern continental slope of Portugal, turning northward around Cape São Vicente [*Ambar*, 1983; *Ochoa and Bray*, 1991]. It cannot be excluded that this Mediterranean vein plays some role in the sea surface slope along the south coast of Portugal. The pressure gradient may result from a positive wind stress curl [*Wang*, 1997; *Bray et al.*, 1999], or from spatial gradients in upwelling intensity, established by spatial gradients in the wind stress field [*Largier et al.*, 1993; *Harms and Winant*, 1998]. In this hypothesis the pressure gradients are formed locally and the coastal warm countercurrent seems to be localized, usually associated with mesoscale features, rather than to constitute any continuous pattern along the coast. The effect of a positive wind curl associated with the sharp protrusion of the Cape São Vicente, may cooperate and enhance the inshore countercurrent in the region, but does not appear to be its primary driving factor.

[61] The coastal warm countercurrent described in this study is seen to extend along all the south coast of Portugal, progressing from the Gulf of Cádiz and turning northward around the Cape São Vicente. It seems to be linked to the body of surface warm water formed in the Eastern part of the gulf. This warm water moves generally west when easterly winds occur in the Gulf and Strait of Gibraltar. On the basis of correlations between sea surface temperatures in different parts of the Gulf and the Strait of Gibraltar, *Folkard et al.* [1997] argue that when the wind at the strait is easterly, cool water upwelled at the southern side of the strait forces this warm water body westward. This mechanism could help establish the observed slope, but cannot explain alone the poleward progression of the narrow coastal warm feature. A strong contribution to the surface tilt can be made by the general eastward drift entering the Gulf of Cádiz. The excess of this that does not enter the Mediterranean accumulates against the eastern coasts near the Strait and recirculates cyclonically along the coast of the Gulf of Cádiz and southern Portugal. This mechanism is strongly supported in a recent paper by *Mauritzen et al.* [2001]. from transport balance considerations to explain the spreading of the high-salinity signal westward in the North Atlantic, the authors need to invoke advection of excess Atlantic Water westward out of the gulf as a shallow flow on the northern side of the Gulf of Cádiz, directly above the Mediterranean outflow. A significant tendency for recirculation within the shallow layers in the gulf is found by the authors through rotating tank experiments, and direct observations in late summer indicate a northward boundary current circulation within the gulf, turning around Cape São Vicente.

[62] The situation found here seems to have some similarity with that off Peru, where the alongshore pressure gradient plays an important role. There, the alongshore velocity field over the shelf and slope is not strongly driven by the local alongshore component of the wind stress, although when wind stress increases in magnitude it gains importance as a driving mechanism [*Brink et al.*, 1978]. Also, in the Southern California Bight, where the winds are generally weak, currents over the shelf are primarily driven by local gradients in adjusted sea level [*Lentz and Winant*, 1986; *Hickey*, 1992]. The warm coastal counterflow feature appears similar to those off California during upwelling relaxation, where spatial variations in the upwelling intensity cause density and related adjusted sea level differences that drive the poleward currents near the coast [*Send et al.*, 1987; *Harms and Winant*, 1998].

9. Conclusions

[63] The analysis of the satellite thermal infrared imagery archive demonstrated the marked seasonality of the coastal ocean in the region of Cape São Vicente. During summertime the west coast is dominated by an almost permanent upwelling regime and associated equatorward flow of cool waters, while the south coast is characterized by the presence over the continental shelf of a warm coastal countercurrent interrupted by upwelling episodes, strong at times. The kinematics of this region is dominated by the interaction of these two regimes where the south and west coast meet.

[64] The westward counterflow along the south coast is driven by an alongshore pressure gradient, whose effect is augmented or diminished by wind forcing. Strong westerly winds are able to provoke coastal upwelling along the south coast and to reverse the alongshore flow.

[65] The equatorward flow off the west coast is driven by the predominant northerly winds that, in accordance with Ekman theory, force near-surface offshore transport. This gives rise to coastal upwelling and to the associated southward current jet, by geostrophic adjustment. During northerly wind relaxations, the warm coastal countercurrent along the south coast turns clockwise around Cape São Vicente and continues northward as much as 120 km along the west coast.

[66] The coastal circulation depends on both the wind stress and the pressure gradient alongshore, whose relative magnitudes govern the direction and strength of the circulation. During the summer off the west coast, the wind stress dominates the pressure gradient, an upwelling regime prevails, and the flow is equatorward for most of the season. An opposed situation occurs off the south coast, where the pressure gradient dominates, the upwelling events are intermittent, and the coastal circulation is mainly westward. Thus, the behaviour of the west coast suggests a pattern typical of an eastern boundary current upwelling system, but this is somewhat modified in the south coast.

[67] The coastal transition zone off Cape São Vicente is the region where the southward current jet of cooler water upwelled off the west coast is no longer bounded by a coast and where it interacts with the warmer coastal counterflow.

Analysis of long series of satellite thermal infrared images revealed the existence of three preferred directions for the continuation of the cool water jet. (1) The most persistent throughout the summer is eastward along the southern shelf break. This eastward cool flow at times merges with waters previously upwelled locally, which become separated from shore by the warmer coastal counterflow. (2) The second preferred direction of spreading occurs less frequently and results in the southward development of a filament. It is fed by colder waters upwelled at Cape São Vicente and farther north and represents the southernmost extent of the intense coastal upwelling jet which overshoots Cape São Vicente. This southward filament develops only after a prolonged west coast upwelling. (3) The least frequent feature to develop is a cool filament that grows westward at the latitude of Cape São Vicente. It appears to result from the meandering of the equatorward jet when it is persistent and intense during the upwelling season.

[68] The coastal countercurrent is seen to interact with the equatorward jet following relaxation of the northerly winds, not only by separating the upwelled water from the coast, but also occasionally, when it is energetic enough, breaking westward offshore through the equatorward cool flow and separating the eastward and southward cool features from the upwelled waters upcoast.

References

Ambar, I., A shallow core of Mediterranean water off western Portugal, *Deep Sea Res.*, *30*, 677–680, 1983.

Ambar, I., and M. R. Howe, Observations of the Mediterranean outflow, 1, Mixing in the Mediterranean outflow, *Deep Sea Res.*, *26*, 535–554, 1979.

Armi, L., and W. Zenk, Large lenses of highly saline Mediterranean water, *J. Phys. Oceanogr.*, *14*, 1560–1575, 1984.

Batteen, M. L., J. R. Martinez, D. W. Brian, and E. J. Buch, A modeling study of the coastal eastern boundary current system off Iberia and Morocco, *J. Geophys. Res.*, *105*, 14,173–14,195, 1999.

Bower, A. S., L. Armi, and I. Ambar, Lagrangian observations of meddy formation during a Mediterranean undercurrent seeding experiment, *J. Phys. Oceanogr.*, *27*, 2545–2575, 1997.

Bray, N. A., A. Keyes, and W. M. L. Morawitz, The California Current System in the Southern California Bight and the Santa Barbara Channel, *J. Geophys. Res.*, *104*, 7695–7714, 1999.

Brink, K. H., and T. J. Cowles, The coastal transition zone program, *J. Geophys. Res.*, *96*, 14,637–14,647, 1991.

Brink, K. H., J. S. Allen, and R. L. Smith, A study of low-frequency fluctuations near the Peru coast, *J. Phys. Oceanogr.*, *8*, 1025–1041, 1978.

Chelton, D. B., Seasonal variability of alongshore geostrophic velocity off central California, *J. Geophys. Res.*, *89*, 3473–3486, 1984.

Chelton, D. B., A. W. Bratkovich, R. L. Bernstein, and P. M. Kosro, Poleward flow off central California during the spring and summer of 1981 and 1984, *J. Geophys. Res.*, *93*, 10,604–10,620, 1988.

Fiúza, A. F. G., The Portuguese coastal upwelling system, in *Actual Problems of Oceanography in Portugal*, pp. 45–71, Junta Nacl. de Invest. Cient. e Tecnol., Lisbon, Portugal, 1982.

Fiúza, A. F. G., Upwelling patterns off Portugal, in *Coastal Upwelling: Its Sediment Record, Part A*, edited by E. Suess and J. Thiede, pp. 85–98, Plenum, New York, 1983.

Fiúza, A. F. G., Hidrologia e dinâmica das águas costeiras de Portugal, Ph.D. thesis, Univ. de Lisboa, Lisbon, Portugal, 1984.

Fiúza, A. F. G., M. E. Macedo, and M. R. Guerreiro, Climatological space and time variation of the Portuguese coastal upwelling, *Oceanol. Acta*, *5*, 31–40, 1982.

Folkard, A. M., P. A. Davies, A. F. G. Fiúza, and I. Ambar, Remotely sensed sea surface thermal patterns in the Gulf of Cádiz and Strait of Gibraltar: Variability, correlations, and relationships with the surface wind field, *J. Geophys. Res.*, *102*, 5669–5683, 1997.

Frouin, R., A. F. G. Fiúza, I. Ambar, and T. J. Boyd, Observations of a poleward surface current off the coasts of Portugal and Spain during winter, *J. Geophys. Res.*, *95*, 679–691, 1990.

Gill, A. E., *Atmosphere–Ocean Dynamics*, Academic, San Diego, Calif., 1982.

Harms, S., and C. D. Winant, Characteristic patterns of the circulation in the Santa Barbara Channel, *J. Geophys. Res.*, *103*, 3041–3065, 1998.

Haynes, R., Eulerian and Lagrangian observations in the Iberian coastal transition zone, Ph.D. thesis, Univ. of Wales, Bangor, U.K., 1993.

Haynes, R., and E. D. Barton, A poleward flow along the Atlantic coast of the Iberian Peninsula, *J. Geophys. Res.*, *95*, 11,425–11,442, 1990.

Haynes, R., E. D. Barton, and I. Pilling, Development, persistence, and variability of upwelling filaments off the Atlantic coast of the Iberian Peninsula, *J. Geophys. Res.*, *98*, 22,681–22,692, 1993.

Hickey, B., Circulation over the Santa Monica–San Pedro Basin and Shelf, *Prog. Oceanogr.*, *30*, 37–115, 1992.

Hickey, B., and N. E. Pola, The seasonal alongshore pressure gradient on the west coast of the United States, *J. Geophys. Res.*, *88*, 7623–7633, 1983.

Hidrográfico, I., *Tabelas de Marés 1997*, M.D.N./Marinha, Lisbon, Portugal, 1996.

Hinrichsen, H.-H., M. Rein, R. H. Kase, and W. Zenk, The Mediterranean water tongue and its chlorofluoromethane signal in the Iberian Basin in early summer 1989, *J. Geophys. Res.*, *98*, 8405–8412, 1993.

Huyer, A., P. M. Kosro, S. J. Lentz, and R. C. Beardsley, Poleward flow in the California Current System, in *Poleward Flows Along Eastern Ocean Boundaries*, edited by S. J. Neshyba et al., pp. 142–156, Springer-Verlag, New York, 1989.

Jungclaus, J. H., and G. L. Mellor, A three-dimensional model study of the Mediterranean outflow, *J. Mar. Syst.*, *24*, 44–66, 2000.

Kelley, K. A., The influence of winds and topography on the sea surface temperature patterns over the northern California slope, *J. Geophys. Res.*, *90*, 11,783–11,795, 1985.

Kosro, P. M., Structure of the coastal current field off northern California during the coastal ocean dynamics experiment, *J. Geophys. Res.*, *92*, 1637–1654, 1987.

Largier, J. L., B. A. Magnell, and C. D. Winant, Subtidal circulation over the northern California shelf, *J. Geophys. Res.*, *98*, 18,147–18,179, 1993.

Lentz, S. J., and C. D. Winant, Subinertial currents in the southern California shelf, *J. Phys. Oceanogr.*, *16*, 1737–1750, 1986.

Mauritzen, C., Y. Morel, and J. Paillet, On the influence of Mediterranean Water on the central waters of the North Atlantic Ocean, *Deep Sea Res., Part I*, *48*, 347–381, 2001.

McClain, E. P., W. G. Pichel, and C. C. Walton, Comparative perfomance of AVHRR-based multichannel sea surface temperatures, *J. Geophys. Res.*, *90*, 11,587–11,601, 1985.

McCreary, J. P., P. K. Kundu, and S.-Y. Chao, On the dynamics of the California Current System, *J. Mar. Res.*, *45*, 1–32, 1987.

Meincke, J., G. Seidler, and W. Zenk, Some current observations near the continental slope off Portugal, *Meteor Forschungsergebnisse A*, *16*, 15–22, 1975.

Miller, P., S. Groom, A. McManus, J. Selly, J. Woolfenden, and L. Osborne, Remote sensing activities in omex, final report, Ocean Margins Exchange Proj. I, Remote Sens. Data Anal. Serv., Plymouth Mar. Lab., Plymouth, UK, 1996.

Ochoa, J., and N. A. Bray, Water mass exchange in the Gulf of Cadiz, *Deep Sea Res., Part A*, *38*, 5465–5503, 1991.

Oey, L.-Y., A forcing mechanism for the poleward flow off the southern California coast, *J. Geophys. Res.*, *104*, 13,529–13,539, 1999.

Pingree, R. D., and B. L. Cann, A shallow meddy (a smeddy) from the secondary Mediterranean salinity maximum, *J. Geophys. Res.*, *98*, 20,169–20,185, 1993.

Prater, M. D., and T. B. Sanford, A meddy of Cape St. Vincent, part i, Description, *J. Phys. Oceanogr.*, *24*, 1572–1586, 1994.

Ramp, S. R., and C. L. Abbott, The vertical structure of currents over the continental shelf off Point Sur, CA, during spring 1990, *Deep Sea Res.*, *45*, 1443–1470, 1998.

Ramp, S. R., P. F. Jessen, K. H. Brink, P. P. Niiler, F. L. Daggett, and J. S. Best, The physical structure of cold filaments near Point Arena, California, during June 1987, *J. Geophys. Res.*, *96*, 14,859–14,883, 1991.

Relvas, P., The physical oceanography of the Cape São Vicente upwelling region observed from sea, land and space, Ph.D. thesis, Univ. of Wales, Bangor, 1999.

Relvas, P., and E. Barton, Poseidon cruise 201/9 report: Physical oceanography data report, technical report, Univ. of Algarve, Faro, Portugal, 1995.

Rhein, M., and H.-H. Hinrichsen, Modification of Mediterranean water in the Gulf of Cadiz, studied with hydrographic and chlorofluoromethanes data, *Deep Sea Res., Part I, 40,* 267–291, 1993.

Richardson, P. L., M. S. McCartney, and C. Maillard, A search for meddies in historical data, *Dyn. Atmos. Oceans., 15,* 241–265, 1991.

Send, U., R. C. Beardsley, and C. D. Winant, Relaxation from upwelling in the coastal ocean dynamics experiment, *J. Geophys. Res., 92,* 1683–1698, 1987.

Sousa, F. M., and A. Bricaud, Satellite-derived phytoplankton pigment structures in the portuguese upwelling area, *J. Geophys. Res., 97,* 11,343–11,356, 1992.

Stammer, D., H. H. Hinrichsen, and R. H. Kase, Can meddies be detected by satellite altimetry?, *J. Geophys. Res., 96,* 7005–7014, 1991.

Strub, P. T., P. M. Kosro, and A. Huyer, The nature of the cold filaments in the California Current System, *J. Geophys. Res., 96,* 14,743–14,768, 1991.

Tychensky, A., and X. Carton, Hydrological and dynamical characterization of meddies in the Azores region: A paradigm for baroclinic vortex dynamics, *J. Geophys. Res., 103,* 25,061–25,079, 1998.

United Nations Educational, Scientific, and Cultural Organization (UNESCO), Processing of oceanographic station data, technical report, Joint Panel on Oceanogr. Tables and Stand., Paris, 1991.

Wang, D.-P., The Strait of Gibraltar Model: Internal tide, diurnal inequality and fortnightly modulation, *Deep Sea Res., Part I, 40,* 1187–1203, 1993.

Wang, D.-P., Effects of small-scale wind on coastal upwelling with application to Point Conception, *J. Geophys. Res., 102,* 15,555–15,566, 1997.

Winant, C. D., R. C. Beardsley, and R. E. Davis, Moored wind, temperature and current observations made during Coastal Ocean Dynmics Experiment 1 and 2 over the northern California continental shelf and upper slope, *J. Geophys. Res., 92,* 1569–1604, 1987.

Wooster, W. S., A. Bakun, and D. R. McLain, The seasonal upwelling cycle along the eastern boundary of the North Atlantic, *J. Mar. Res., 34,* 131–141, 1976.

Zenk, W., On the Mediterranean outflow west of Gibraltar, *Meteor Forschungsergeb, Reihe A, 16,* 23–34, 1975.

Zenk, W., and L. Armi, The complex spreading pattern of Mediterranean water off the Portuguese continental slope, *Deep Sea Res., Part A, 37,* 1805–1823, 1990.

––––––––––––––––

E. D. Barton, School of Ocean Sciences, University of Wales, Menai Bridge LL59 5EY, UK. (oss041@bangor.ac.uk)

P. Relvas, Centro de Investigação Marinha e Ambiental, Universidade do Algarve, Campus de Gambelas, 8000-117 Faro, Portugal. (prelvas@ualg.pt)